603589

COPY 2 of 3 COPIES

NRL REPORT 1223

101p
hc-4.00
mf-0.75

THE PROBLEM

Measure the characteristics of boundary layer turbulence for water flowing through pipes under controlled laboratory conditions. Study the character of turbulence components and the nature of water flow noise by harmonic and numerical analysis of experimental measurements. Compare the findings with existing knowledge of airflow and with theoretical analyses and computations of flow noise. Derive a method for approximating water flow noise values for a range of conditions.

RESULTS

1. The water pipe flow study gave experimentally derived values of pipe wall pressure fluctuations, radial pipe deflections at one point, and pressure-head variation along the pipe, for turbulent flow rates from 0.65 to 9.6 fps with the experimental test pipe section insulated from external noise sources.

2. Test pipe material, test pipe length, and location of the measurement points (hydrophone location, etc.,) did not influence the measured values.

3. The broadband fluctuating pressure at the pipe wall depends directly on the dynamic pressure and somewhat on the Reynolds number as related by the relation $p/q = k^2\ 0.079/R^{.25}$. The value of k (the velocity ratio of fluctuating radial stress to the wall shear stress in the constant stress region) averaged 0.9 for the experimental data.

4. Based upon analysis of 232 spectra curves, the shapes of the curves are nearly identical and are of the form expected from theory. Before the peak, the slope of

the curves is about 1.0, and after the peak, in the equilibrium region, the slope is about -1.66, resembling the Kolmogoroff-region slope of the kinetic energy spectrum.

5. The position of the peak of the spectra curves depends upon the flow conditions. Based upon study of 232 spectra, the position corresponds to a Strouhal number of 0.49 and to a wave number of 150 feet^{-1}.

6. Spectral measurements with the micrometer set, with very thin pipe wall thicknesses, approximated hydrophone measurement spectra.

7. Numerical analysis of photographed waveforms produced autocorrelations and power spectra. Spectra from the numerical analysis agreed with those from third-octave analysis. The Taylor microscales of turbulence are of the same order of magnitude obtained for air flow by other experimenters.

8. The dissipation values for water flow, based upon wall shear stress measurements, are of the same order of magnitude as Laufer's values for air flow.

RECOMMENDATIONS

1. Apply the derived method for approximating the magnitude of broadband fluctuations to experimental, developmental, and service use.

2. For research purposes, use test hydrophones which resemble those used in actual service applications.

3. Continue pipe-flow "water tunnel" experiments as an efficient method for studying water flow noise and turbulence. Study higher flow rates and response frequencies

under the type of laboratory conditions described herein. Study application of experimental findings to component and system development.

ADMINISTRATIVE INFORMATION

Work described herein was performed under SR 011 01 01, Task 0401 (NEL Z1-21) by the Listening Division. This report covers intermittent work from 1958 to February 1963. The report was approved for publication 13 May 1964.

CONTENTS

TABLES

ILLUSTRATIONS

ILLUSTRATIONS (Continued)

LIST OF SYMBOLS

B..... bulk modulus of elasticity
C..... specific heat
c..... velocity of sound in the medium
D..... pipe inside diameter
e..... internal energy per unit mass
f..... wall friction factor
f'..... Blasius' relationship between the friction coefficient, f, and the Reynolds number; $F = 0.079/R^{.25}$
$F(0)$..... is the dc component, which must be finite (dc is defined by $n = 0$)
F_t..... external force per unit mass
$F(N)$..... complex constant of a series
$|F(n)|^2$ ... power spectrum of $f(t)$
$F(\omega)$ ..... Fourier transform of $f(t)$
f..... friction coefficient (τ_w/q)
f_t..... chosen frequency interval
$f(t)$..... periodic function
$G(f)$..... power spectrum based on only positive frequencies
h..... enthalpy per unit mass
k..... velocity ratio of fluctuating radial stress to wall shear stress in the constant stress region
k..... wave number, equal to $2\pi u/\overline{u}$
L..... length
ℓ..... representative dimension
n..... frequency
P..... hydrostatic pressure
P..... rms broadband pressure
P_n..... power spectrum
p..... measured rms broadband pressure
$p(t)$ ..... wall pressure fluctuation
q..... dynamic head, equal to $\frac{1}{2}\rho\overline{u}^2$
q_t..... heat conducted per unit volume
R..... Reynolds number, equal to $\overline{u}D/\nu$
R..... Reynolds number, equal to $\overline{u}D\rho/\mu$
R..... wall Reynolds number, equal to $x_2\overline{u}/\nu$
$R(\tau)$ ..... autocorrelation between fluctuating radial pressures displaced by time lag τ

LIST OF SYMBOLS (Continued)

r..... pipe radius, inside dimension
S..... Strouhal number, equal to $nr/\bar{u}$
s..... entropy per unit mass
T..... temperature
T_1..... fundamental period
t..... time
U..... maximum mean velocity
U_m..... maximum mean flow velocity
u..... velocity
$\bar{u}$..... mean, average flow velocity (weight flow)
u'..... fluctuating velocity component
u_r..... fluctuating radial turbulent velocity
u_x..... fluctuating longitudinal turbulent velocity
u_φ..... fluctuating tangential turbulent velocity
u_*..... friction velocity
V..... representative velocity
x..... distance
x_2..... wall distance (distance inward from pipe inner wall)
α..... coefficient of volume expansion
Δ ..... dilation, or volume change per unit volume
ΔP..... differential pressure or pressure drop
δ..... boundary layer thickness
δ_{ij}..... Kronecker delta
ϵ..... mean strain
ϵ'..... dissipation per unit mass
μ..... fluid dynamic viscosity
ν..... kinematic viscosity equal to μ/ρ
$\dot{\nu}_{ij}$ ..... strain rate in shear
π..... constant
ρ..... fluid density
σ..... mean stress
σ_{ij}..... stress
σ_{rr}..... fluctuating component of normal stress
τ..... wall shear stress, equal to $\Delta Pr/L2$
τ..... time lag
τ_1..... chosen time interval
τ_w..... wall stress
τ_{ij}..... shearing stress
ψ..... energy dissipation per unit volume

INTRODUCTION

This report covers a continuation of basic research initiated by C. N. Miller of the Navy Electronics Laboratory to study water flow noise. These studies have included experiments with streamlined bodies falling through water, to show that measured laminar flow noise values would be less than turbulent flow values. The falling body noise experiments were conducted with 19 laminar test bodies, at Lake Pend Oreille, Idaho, and were completed in December 1962.[1]*

Experimental studies of noise produced by the flow of water through pipes have been performed at Northwestern University and at the U. S. Navy Experiment Station, Annapolis, Maryland.** However, these studies were not concerned with the nature of flow noise, but rather were designed to show the sum total noise in piping systems.

The pipe flow experiment described in this report was devised for the study of flow noise produced by forcing water through brass, plastic, and glass pipes at controlled rates, under laboratory conditions. Flow rates of 0.65 to 9.6 fps were obtained without extraneous noise, and accurate flow noise measurements were made.

---

*Superscript numbers refer to the list of references at the end of this report.

**This activity is now designated the U. S. Navy Marine Engineering Laboratory.

WATER PIPE FLOW NOISE EXPERIMENT

The objective of the experiment was to produce water pipe flow noise over a range of flow rates through pipe of different materials, under controlled conditions, and to collect, for further processing and analysis, three basic measurements related to the nature of boundary layer turbulence. These measurements were: 1) hydrophone pickups, 2) pipe wall fluctuations, and 3) pressure differential along the boundary layer.

INSTRUMENTATION

The experiments were conducted in a concrete-floored building remote from industrial and traffic noise and vibration. The building provided space for a 65-foot-long straight and level pipe run, and had separate rooms to help isolate the test pipe section from the sound of equipment elsewhere in the building.

Fresh water was stored in a pressure tank, and entered the test pipe section through a globe valve and a 30-foot straight-line assembly of soft rubber tubing and special fittings (fig. 1). The tubing was used to eliminate conduction of noise and vibration to the test pipe section. A manometer, calibrated in pounds of water flow per minute, was installed across a 3-inch to ½-inch reducer between sections of rubber tubing, to function as a venturi flow gauge. The reducer and other fittings and connections in the water line were specially designed and fitted to minimize flow disturbances.

Figure 2 shows a typical test setup. The water storage tank was pressurized through rubber tubing from a zero- to 100-psig controllable external air supply to regulate the water flow rate through the test pipe. The test pipe section, located in a separate room with measuring and recording equipment, was connected to input and output ½-inch ID soft rubber tubing by special tapered fittings to

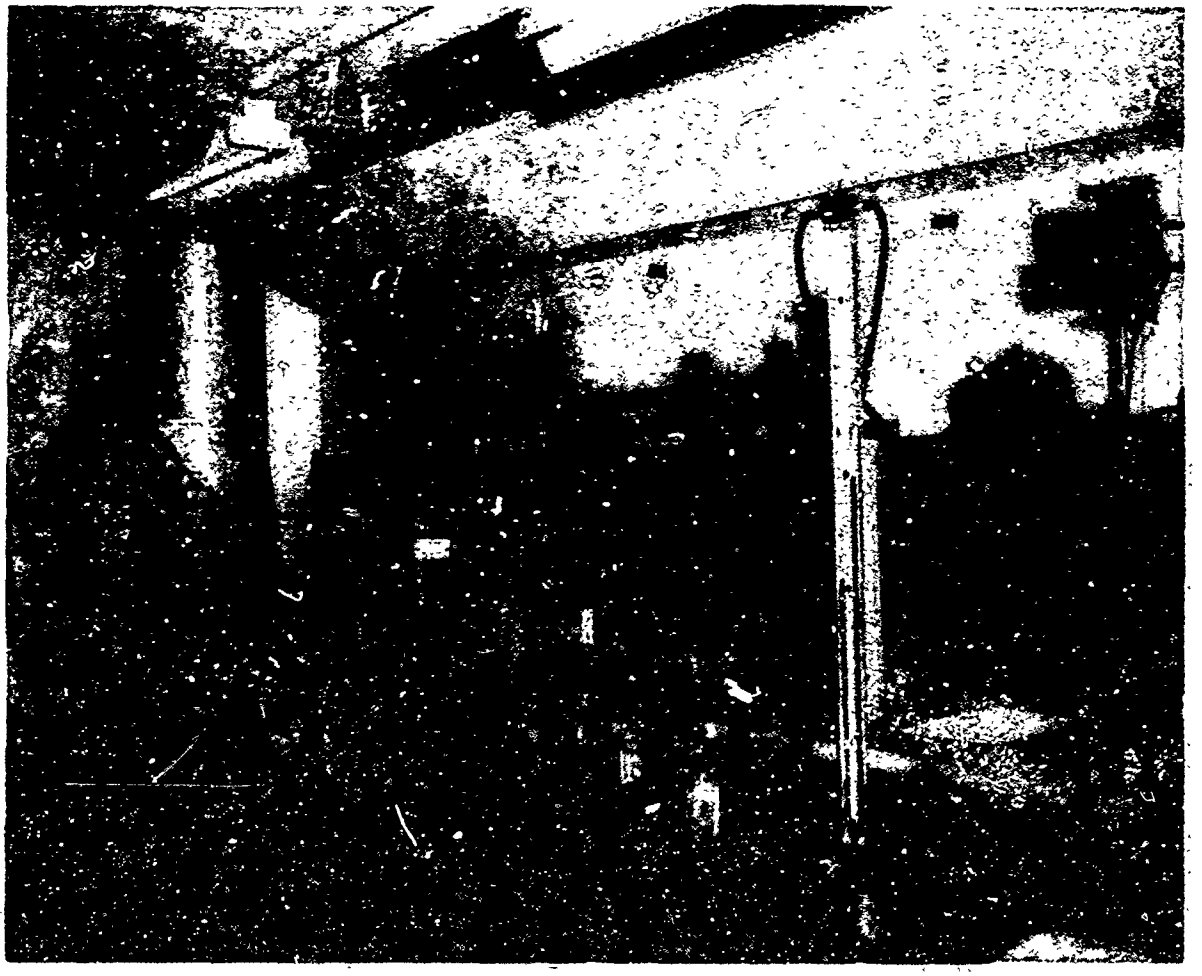

Figure 1. Input section of water pipe flow noise experimental setup.

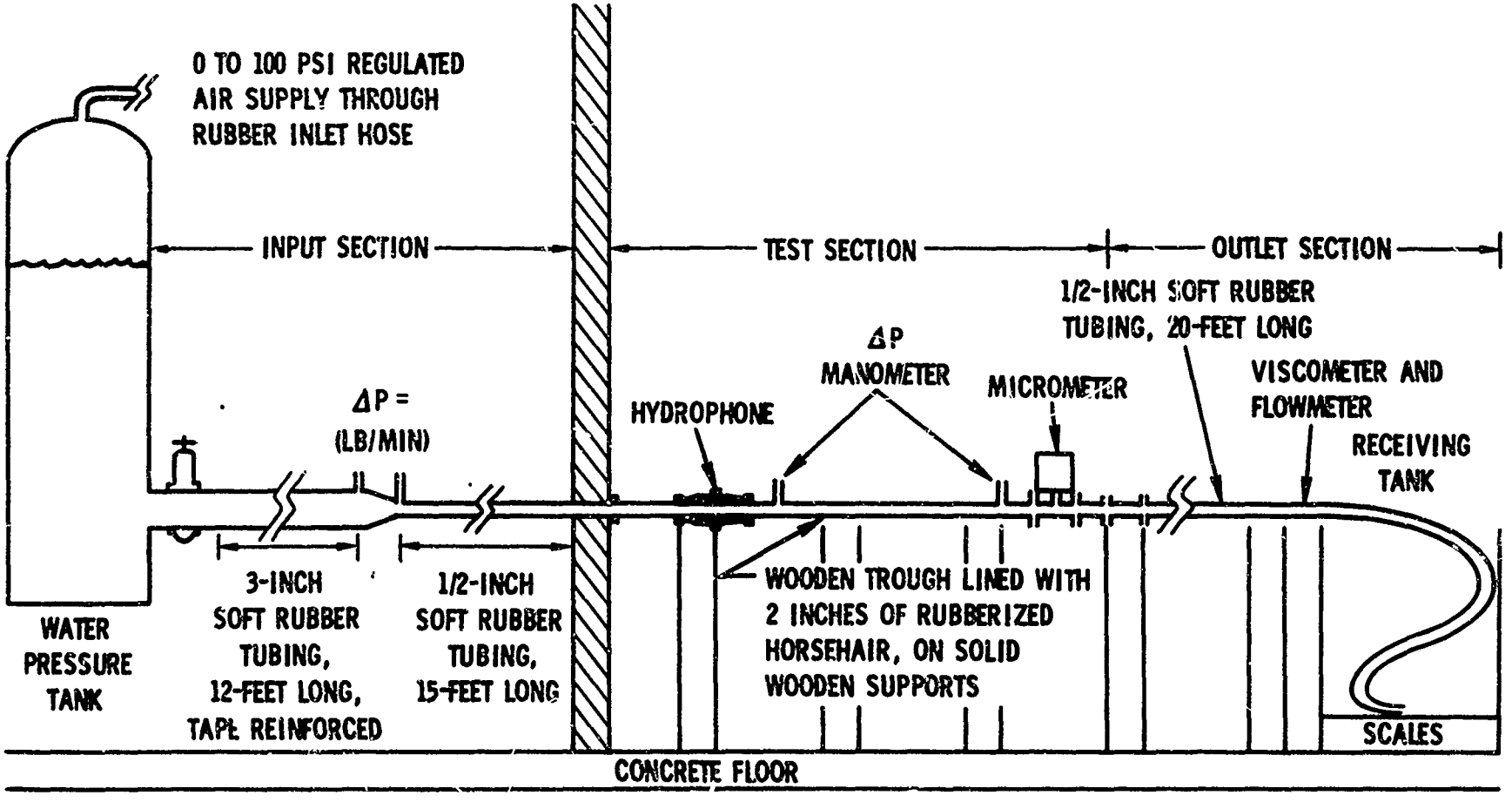

Figure 2. Typical water flow test setup.

maintain a constant inside diameter. The output tubing led into and was coiled down inside a collection tank installed on Fairbanks Morse platform scales. A viscometer and a float-type flowmeter were inserted in the rubber outlet line near the receiving tank.

The test pipe section was of several configurations, comprising 3/8-inch pipe of either glass, brass, or polyvinyl chloride high-impact plastic. Test sections were supported on 2 inches of rubberized horsehair acoustic padding in a solidly supported wooden trough. The pipe selected for the experiments had an inside diameter of 0.494 inch and a wall thickness of 0.09 inch. The test pipe section was instrumented with either of two types of test hydrophones and with an electronic micrometer to measure radial pipe wall fluctuations. Plastic and brass test pipe sections were drilled at two points to provide differential-pressure manometer taps to measure shear pressure drop.

The hydrophone elements were installed flush with the inner walls of the test pipe sections, using special adapters. The smaller-area hydrophone was a barium zirconium titanate bimorph bender 0.37 inch long and 0.1 inch circumferentially. The other was a radially polarized barium titanate ceramic cylinder 0.45 inch long and 0.494 inch ID, mounted flush inside a brass adapter fitting. Details of hydrophone design and calibration are contained in Appendix A.

The electronic micrometer (Micrometer Set, Mutual Inductance, AN/USM-43) was rigidly mounted to 10-inch-long test pipe sections which had been thinned in that area to 0.003-inch wall thickness. The micrometer probe was inductively coupled to a flat metallic surface on the pipe to measure fluctuations in the separating distance as small as 10^{-7} inch. (A flat brass disc was cemented to the plastic pipe to enable inductive coupling. The micrometer was not used with the glass pipe.)

The hydrophone was connected through a preamplifier, amplifier, and attenuator to a Tektronix 512 oscilloscope,

a Magnecord P-60 single-channel tape recorder, and a voltmeter. A Hewlett Packard 20 c/s to 5 kc/s oscillator and a General Radio random noise generator were connected to the recorder and oscilloscope through an attenuator and the preamplifier channel. The mutual inductance micrometer set was connected directly to the oscilloscope, recorder, and voltmeter.

Arrangement of the readout and recording equipment, shown in figure 3, allowed simultaneous visual display and recording of alternate hydrophone, micrometer, time-reference, and random noise signals.

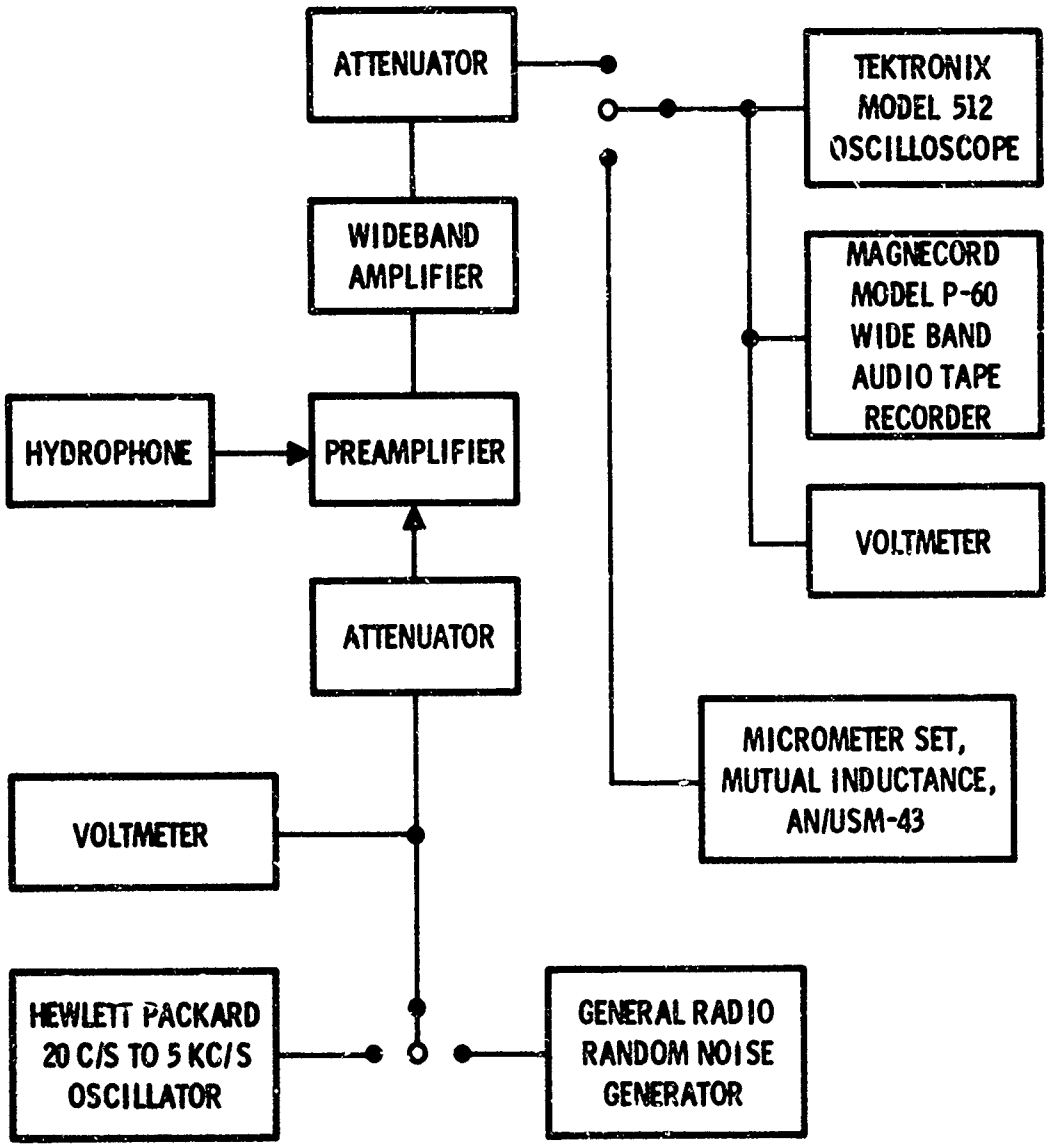

Figure 3. Instrumentation setup.

PROCEDURE

The storage tank was filled with fresh water and pressurized from a constant compressed air supply at a predetermined regulator setting corresponding to a given water flow rate. Zero-flow hydrophone-circuit ambient noise, oscillator, and white-noise generator calibration reference signals were alternately tape-recorded (the recorded zero-flow ambient noise was no greater than the theoretical circuit noise value computed for the hydrophone-amplifier circuit).

The water collection tank drain was closed and the water storage tank outlet globe valve was opened. As water flowed through the test section, visual readings of water temperature, viscosity, flow rate, and shear pressure drop were recorded on data sheets. Micrometer, hydrophone, oscillator, and random-noise generator signals were alternately tape recorded. For each configuration of the test pipe section (table 1) test runs were conducted over a range of flow rates, and measurements and reference signals were recorded for each run.

TABLE 1. WATER FLOW TEST CONFIGURATIONS

Pipe Material	Pipe Length	Instrumentation
PVC Plastic	10 feet	Hydrophone, Micrometer, Manometer
	3 to 30 feet	Manometer
Brass	10 feet	Hydrophone, Micrometer, Manometer
	3 to 30 feet	Manometer

Accurately controlled water flow from 2.79 to 50 pounds per minute was achieved, giving mean average flow rates over the range shown in table 2 (to achieve the lower flow rates, the outlet tubing was constricted between the test pipe section and the collection tank).

TABLE 2. WATER FLOW THROUGH 0.494-INCH ID PIPE*

Pounds Water/Minute	2.79	10.0	20.0	30.0	40.0	50.0
Flow, Feet/Second	0.56	2.005	4.01	6.015	8.02	10.025
Flow, Knots	0.332	1.187	2.374	3.561	4.748	5.935

*Based on fresh water at 60°F, with a density of 62.422 pounds per cubic foot.

Water flow boundary layer turbulence was observed in the glass pipe over the range of flow rates, using a lens system and a bright light to illuminate suspended particles.

DATA REDUCTION

Raw data were recorded on 125,000 feet of broadband audio tape. These data were reduced to quantitative form in several ways, and were integrated with numerical records from the corresponding data sheets of each run, for analysis and study of the characteristics of the flow noise. The experiment provided necessary data to derive autocorrelations; power spectra, broadband magnitudes, and spectrum levels in several ways; and boundary layer wall shear measures of energy dissipation.

A Polaroid camera attached to the oscilloscope photographed the hydrophone and micrometer signal patterns (fig. 4). These patterns were analyzed by Fourier methods to derive power spectra and autocorrelations.

The audio tapes were played back through a Sanborn broadband amplifier/recorder to give graphic analog traces of rectified rms hydrophone and micrometer signal

amplitudes, together with oscillator and random noise reference signal traces. The broadband recordings were also sorted into selected third-octave filter channels of a Sanborn Model 150 six-channel recorder and an NEL third-octave digital analyzer. These provided analog traces of rms values against an accurate time scale, and digital printout of one-cycle bandwidth dB values.

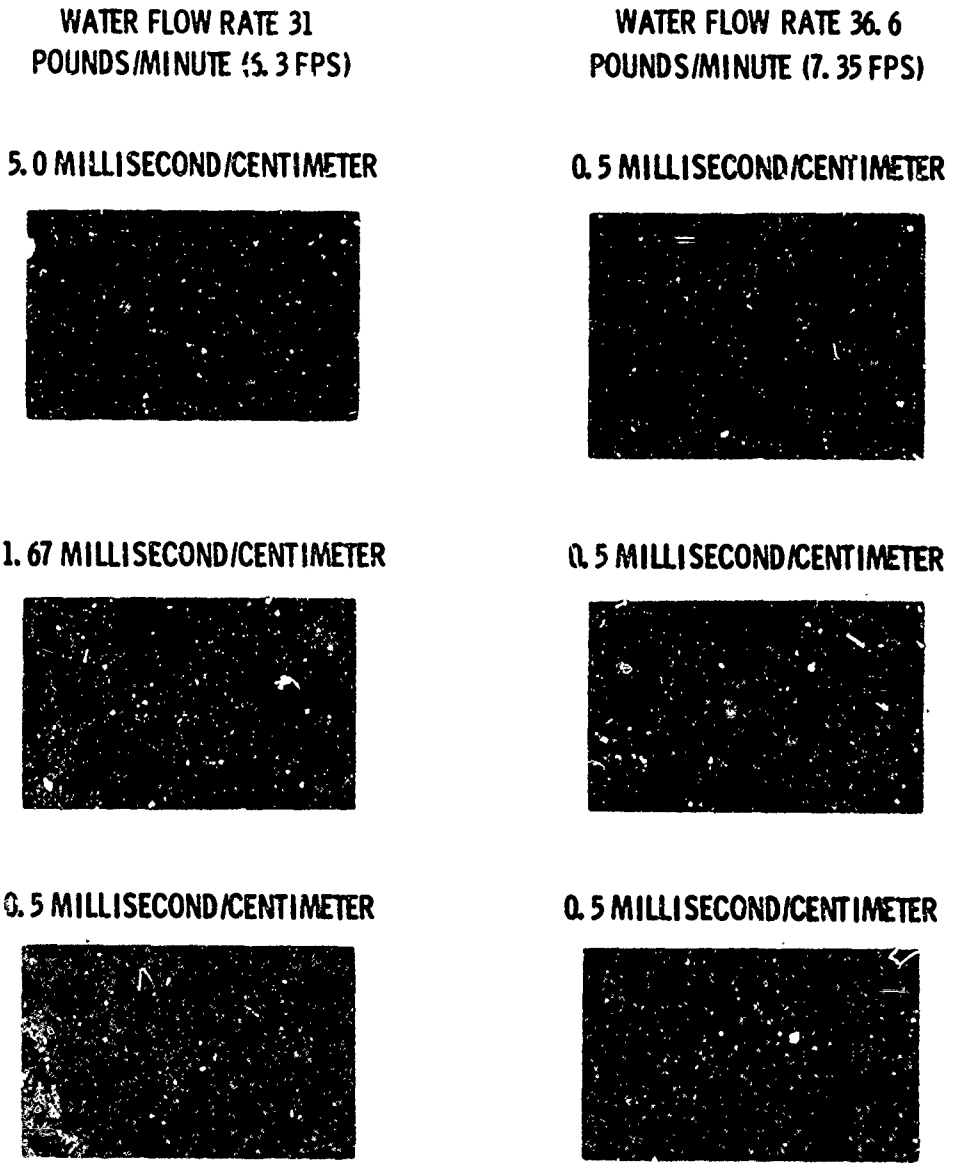

Figure 4. Photographed oscilloscope tracings of broadband audio signals from cylindrical hydrophone pickups of water flow noise in plastic pipe.

DATA ANALYSIS AND PRESENTATION

Results of the water pipe flow experiments were reduced to several graphic forms from which representative data were selected for correlation, analysis, and presentation. Polaroid photos, broadband rectified rms analog traces, single-channel rms dB analog traces, single-cycle bandwidth rms dB values in digital printouts, and numerical records from data sheets were used in numerical and harmonic analyses. Results of the analyses are discussed briefly and presented in graphic form. Theory and methods used in the analyses are presented in Appendix B. Conclusions and recommendations are presented in a following section.

The characteristics of turbulent flow are generally defined by characteristic lengths, correlation functions, characteristic velocities, and by spectrum components. The nature of flow noise, in this case the measured pressure fluctuations at the pipe wall, can also be related in terms of the same types of variables. The one-point hydrophone and micrometer measurements furnished broadband and spectrum levels, and the broadband magnitudes are shown to be related to the velocities.

AUTOCORRELATIONS

Autocorrelations of pressure components were measured at the same point of the pipe wall, and in the same radial direction, but differ in their time separation. The autocorrelation is a periodic function of time lag, and is a Fourier transform of the power spectrum. The Polaroid photos of sound pressure waves were used for numerical evaluation of the autocorrelations. Results are shown in figures 5 and 6.

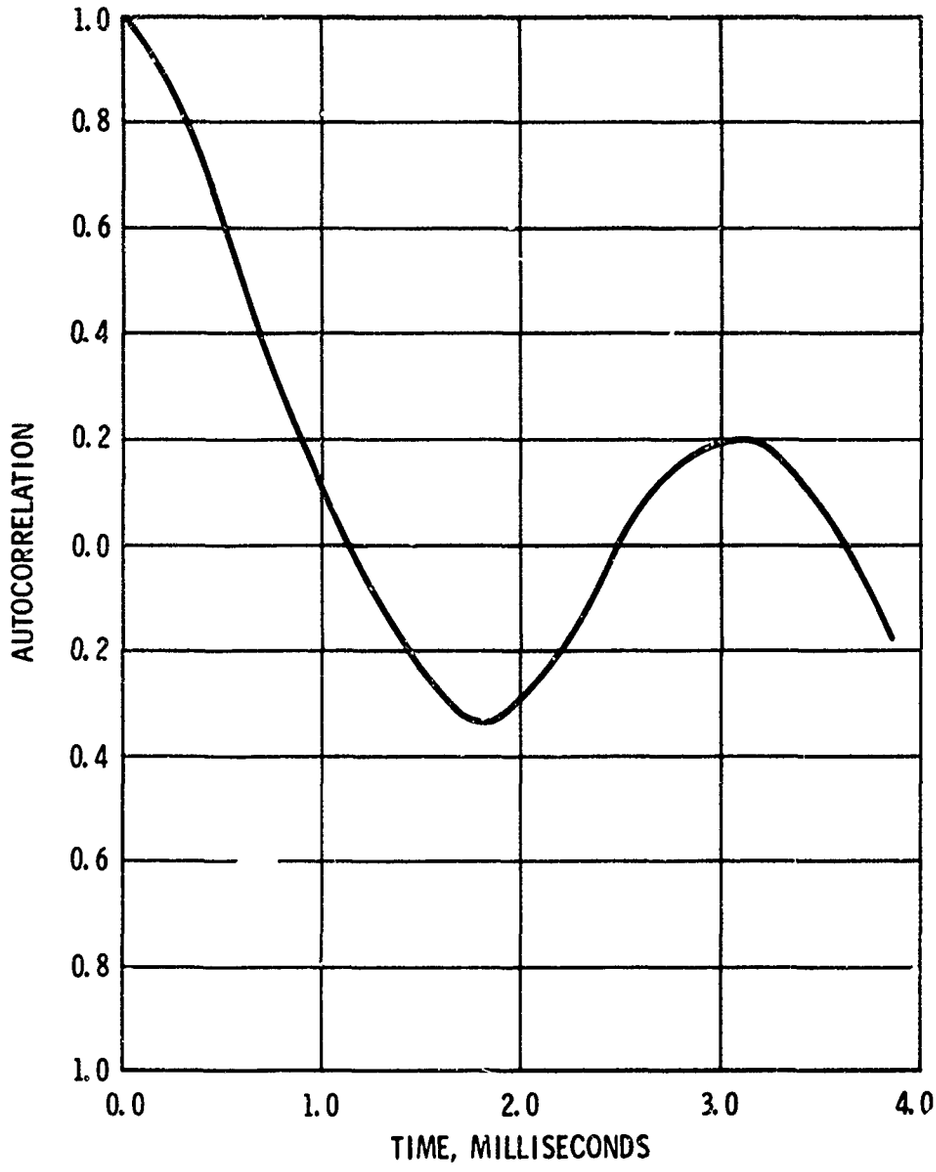

Figure 5. Autocorrelation of wall pressure fluctuations, calculated from oscilloscope photos for 7.32 fps flow rate.

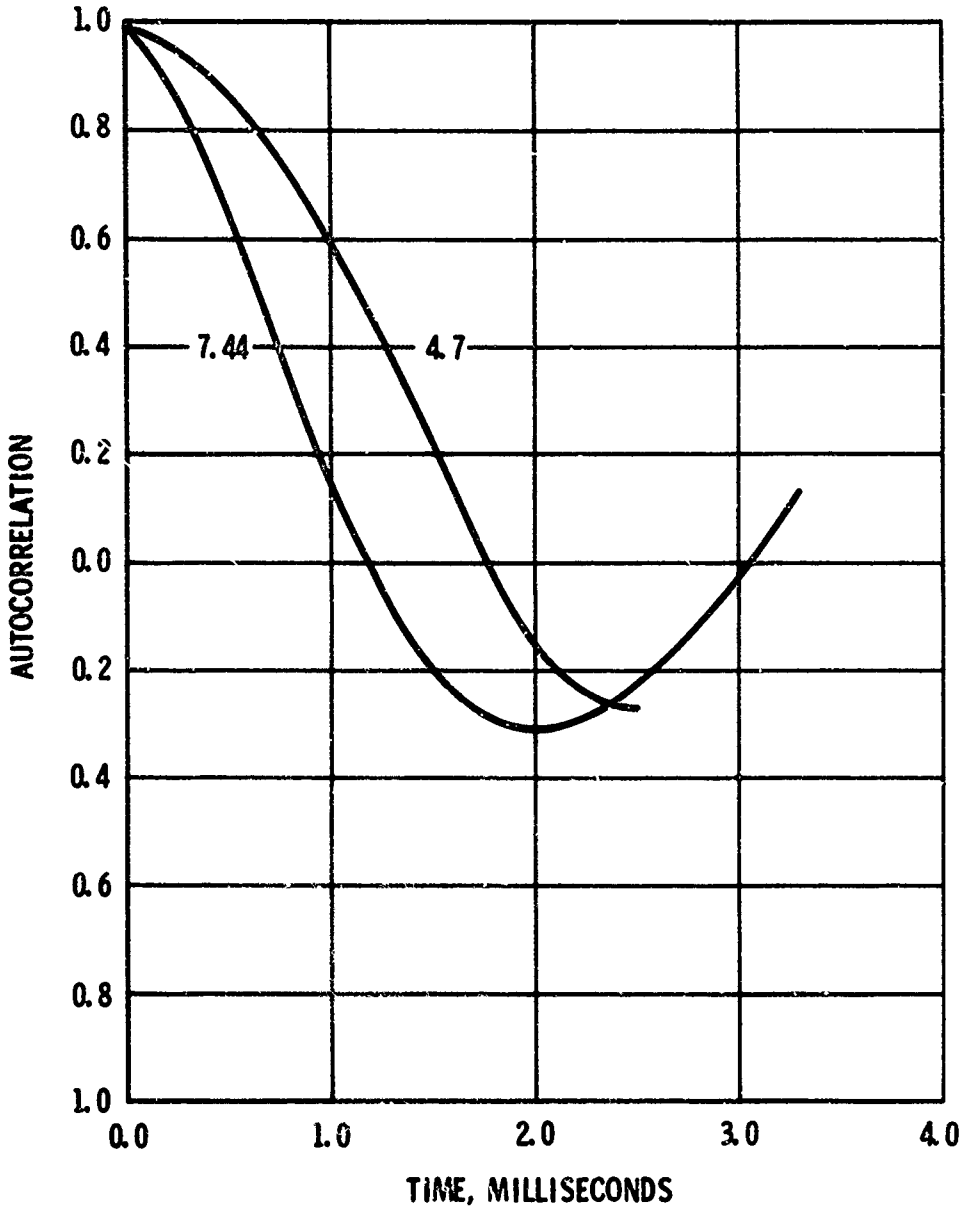

Figure 6. Autocorrelations of wall pressure fluctuations, calculated from oscilloscope photos for 4.7 and 7.44 fps flow rates.

POWER SPECTRA

Spectrum levels were obtained from Sanborn analog records, TODA digital printouts, and by numerical analysis of the Polaroid photos. Figures 7 and 8 show representative measured spectra for the two types of hydrophones and for brass and plastic pipe. The curves show pressure level plotted against wave number. Approximately 232 spectrum curves of pressure fluctuations were obtained from experimental recordings. The shapes of these curves vary, but have fairly constant rising and falling slopes and wave numbers of their peaks. The average rising slope is 1.0, and the average falling slope is 1.65: this is nearly equal to the Kolmogoroff slope of -5/3.

Figures 9 and 10 give spectrum levels of pressure calculated from the photographs, for various flow velocities with both types of hydrophones. These curves are of the same shape and peak at about the same wave numbers as the curves from the Sanborn and digital analyzer records. For low flow rates, the curves from either source rise and fall less steeply than on curves for higher flow rates (at the low flow rates, the Reynolds numbers may be too low for the inertial subrange -- in which the flow is determined solely by the dissipation rate -- to occur).

Figures 11 and 12 show spectrum curves of pipe wall fluctuations from the micrometer measurements. The rise and fall rates are generally less than for hydrophone signal curves. This may result from pipe wall stiffness limiting the correlation distances to small values. Sharper correlation curves tend to produce larger high-frequency components in the system, and they tend to flatten the spectrum curves.

Spectrum curves for the experimental data peak with a mode near the wave number of 150 feet^{-1}. The ordinates of the spectrum curves can also be in terms of the nondimensional Strouhal number, $S = nr/\overline{u}$, where r is the pipe radius, $\overline{u}$ is the mean average flow velocity, and n is the frequency.

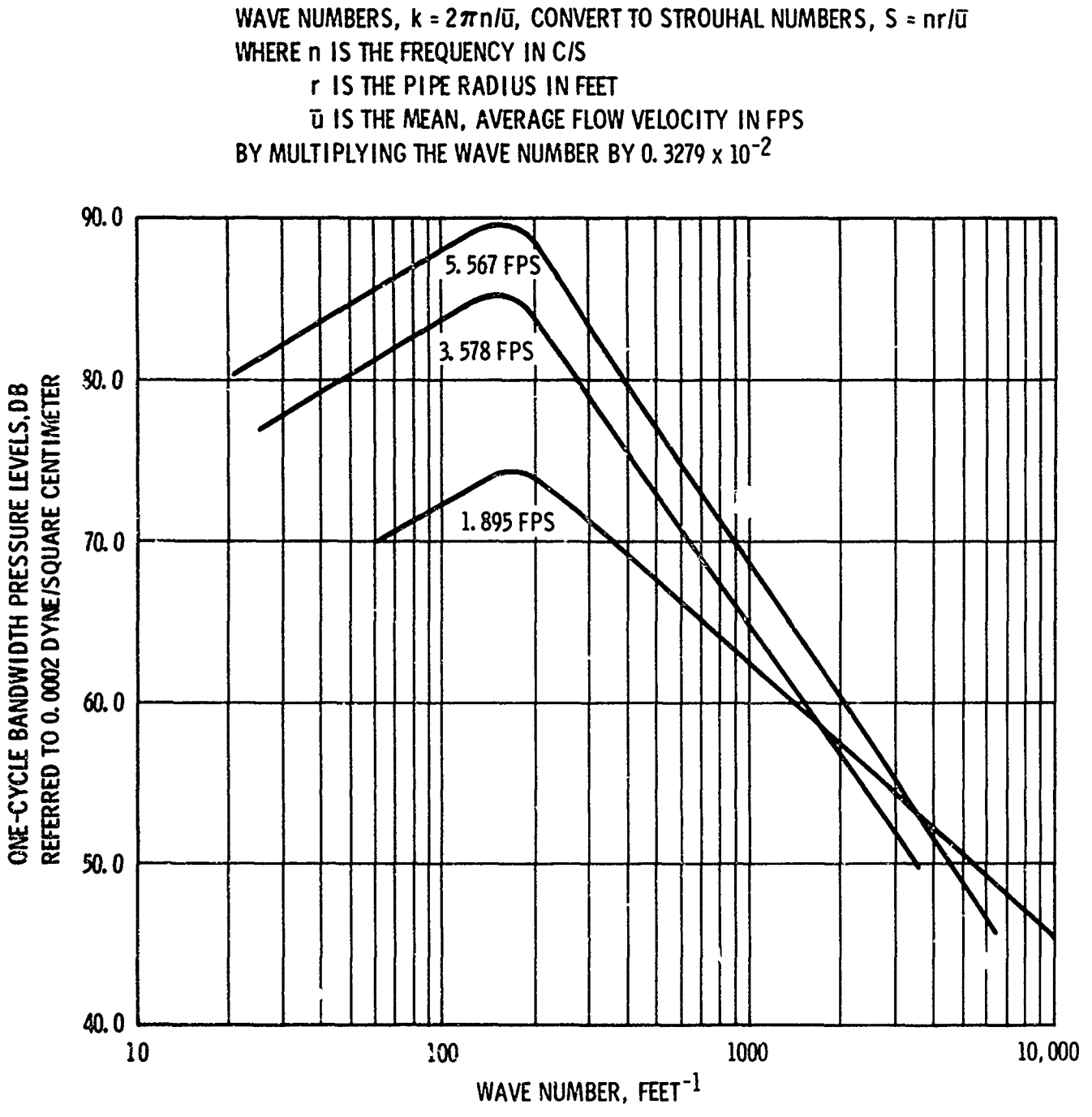

Figure 7. Cylindrical hydrophone sound power spectrum with brass pipe flow.

WAVE NUMBERS, $k = 2\pi n/\bar{u}$, CONVERT TO STROUHAL NUMBERS, $S = nr/\bar{u}$
WHERE n IS THE FREQUENCY IN C/S
r IS THE PIPE RADIUS IN FEET
$\bar{u}$ IS THE MEAN, AVERAGE FLOW VELOCITY IN FPS
BY MULTIPLYING THE WAVE NUMBER BY 0.3279×10^{-2}

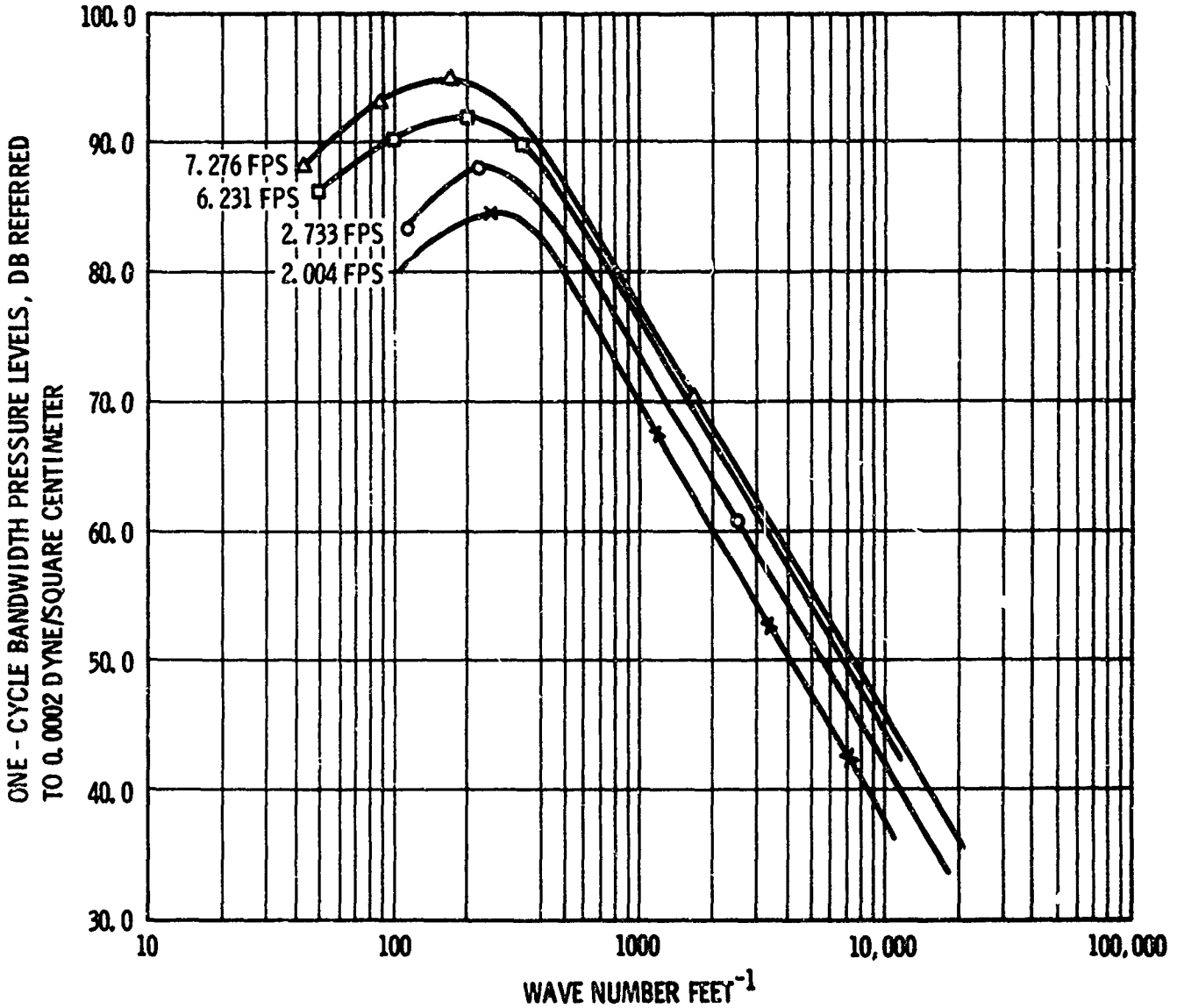

Figure 8. Bimorph hydrophone sound power spectrum with plastic pipe flow.

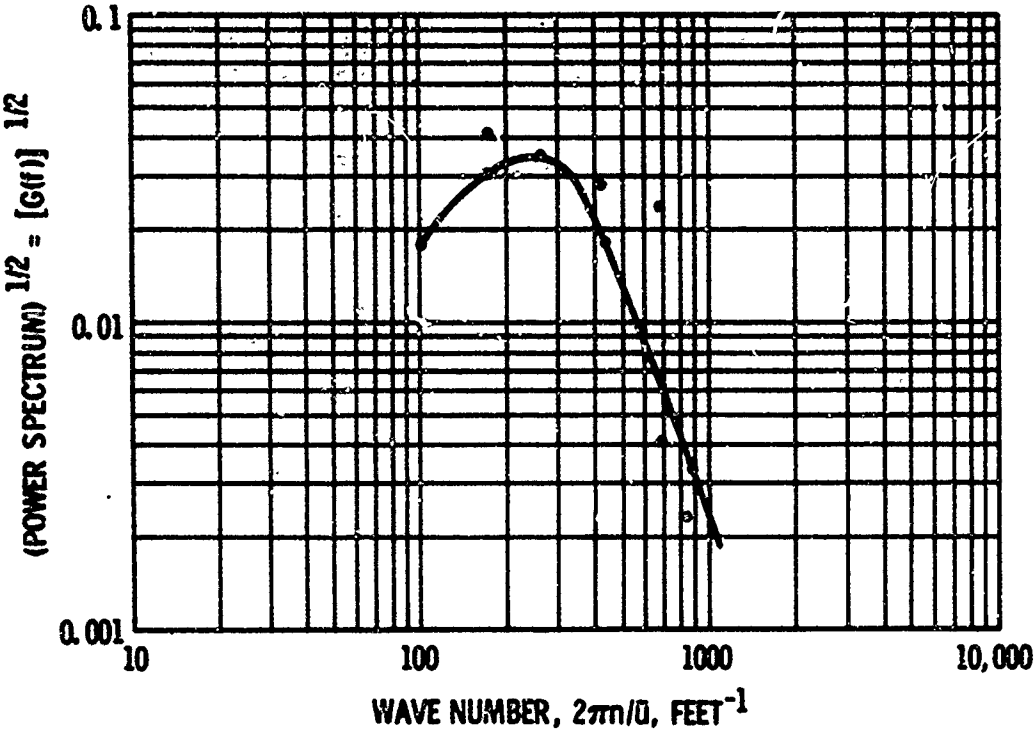

Figure 9. Power spectrum of wall pressure fluctuations, calculated from oscilloscope photos for 7.44 fps flow noise.

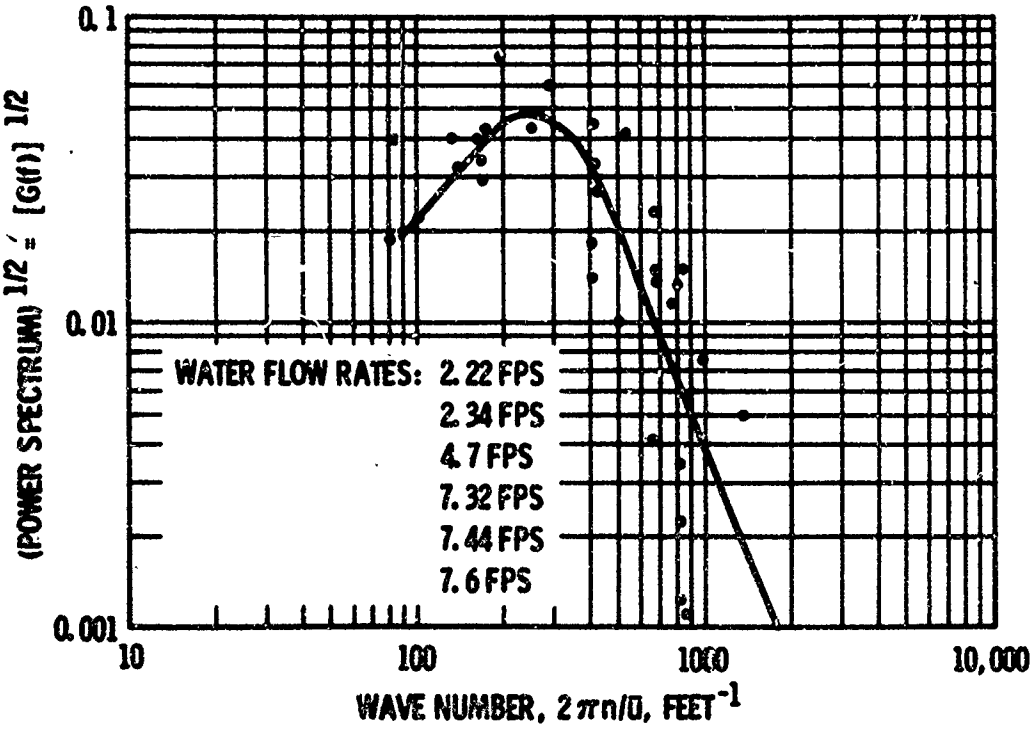

Figure 10. Power spectrum of wall pressure fluctuations, calculated from oscilloscope photos of flow noise for several flow rates.

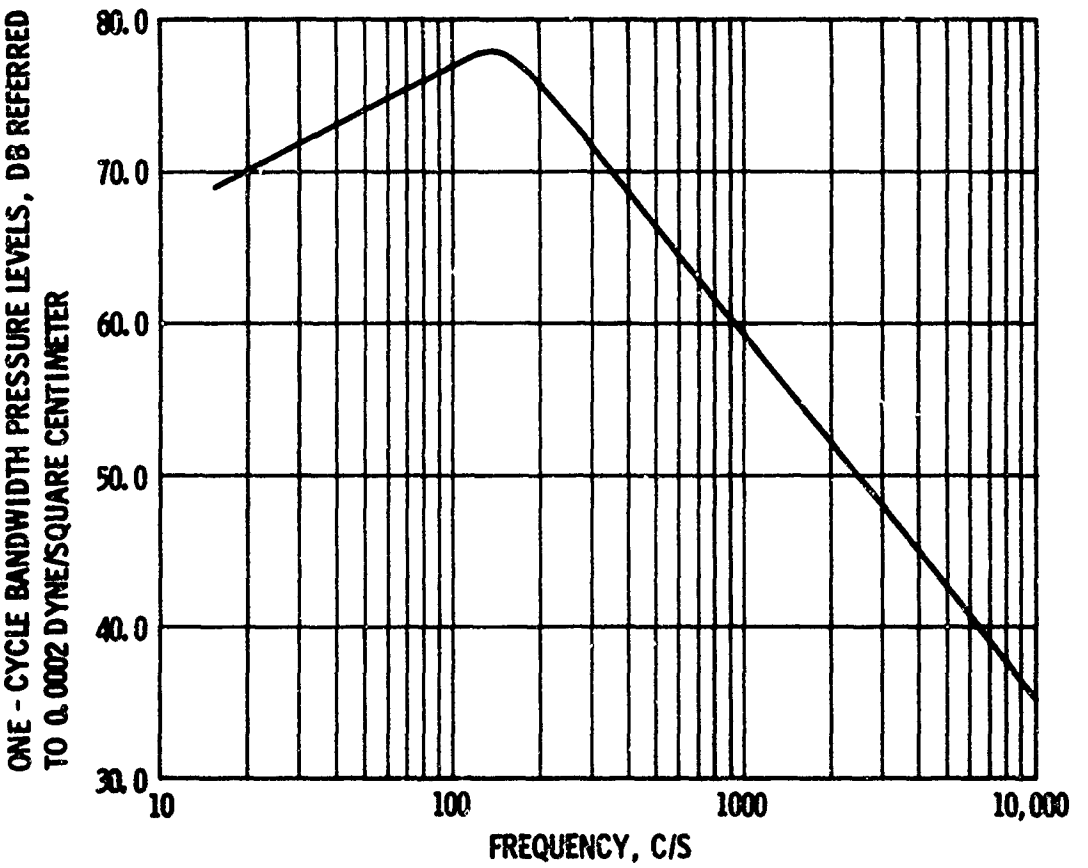

Figure 11. Micrometer signal power spectrum for flow rates of 2.36, 4.52, and 7.46 fps through plastic pipe.

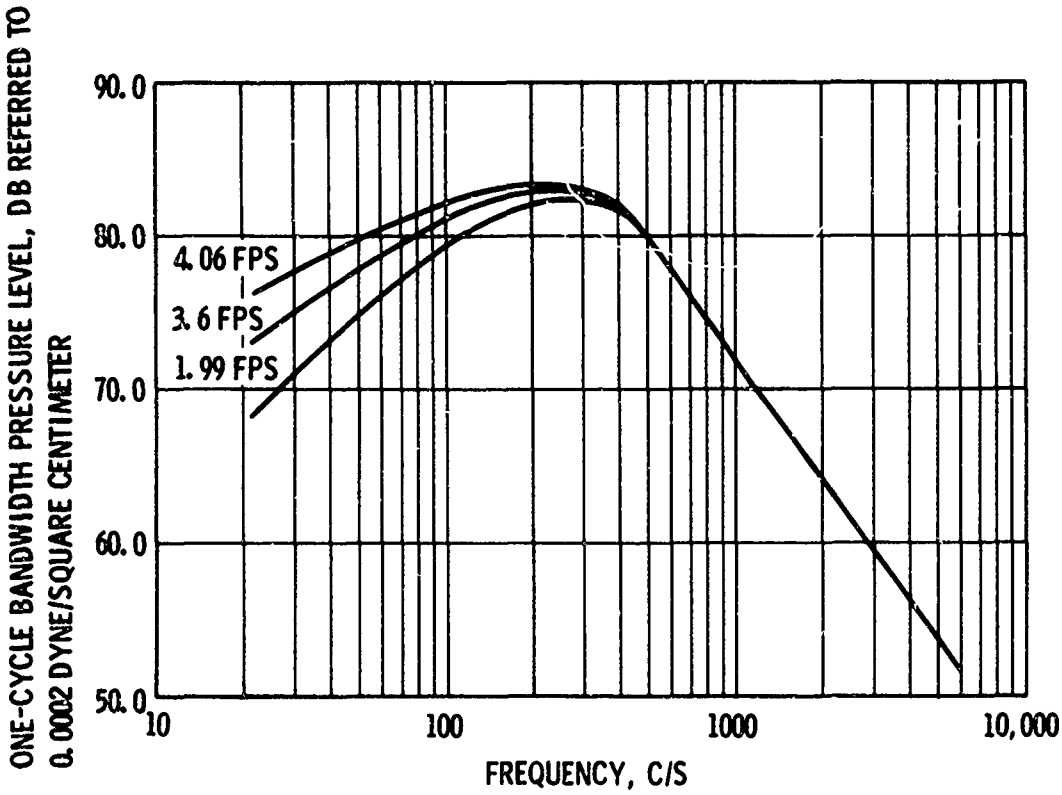

Figure 12. Micrometer signal power spectrum for flow rates of 1.99, 3.6, and 4.06 fps through brass pipe.

Multiplying the wave numbers of figures 7, 8, 9, and 10 by 0.3279×10^{-2} will give the equivalent Strouhal number for the 0.494-inch ID experimental pipe.

The maximum of the spectrum corresponds to the average size of the energy-containing eddies, and the eddy size is proportional to the pipe size. The spectral maxima should occur at the same Strouhal number for pipes of different size, since both eddy sizes and Strouhal numbers are proportional to the pipe diameter. When the spectra are plotted in terms of the Strouhal number, the peak should occur at $S = 0.49$, based on the median peak value of 150 $feet^{-1}$ in wave number. The ratio of the pipe diameter to the eddy size for this wave number is 6.18.

The spectrum curves are plotted in the same dimensions as the kinetic energy spectrum plots of Laufer, Schubauer, Taylor, Klebanoff, and others. The pressure spectrum is of the same dimensions as the energy spectrum. Figure 13 compares a Laufer spectrum curve with one from this study, with the curves plotted against Strouhal number. The curve from this study has a wave number of 120 $feet^{-1}$ at the peak, and the Laufer curve has a wave number of 0.2 centimeter at the peak. Laufer used a 9.72-inch ID pipe, and his wave numbers convert to Strouhal numbers by multiplying by 1.965. The Laufer curve is for the radial-direction kinetic energy spectrum as measured at a distance of 0.691 radius from the pipe wall. The curve Laufer measured nearest the wall is flatter than other Laufer curves and most of the curves from the water pipe flow study (probe measurements are not as accurate near the wall). The Laufer curve and the curve from this study are similar, and both peak at Strouhal number 0.393.

The pressure spectrum curves from this study resemble the energy spectrum curves of contemporary fluid mechanics. The slopes of rise and fall about the maximum are nearly those expected from the theory of isotropic turbulence.

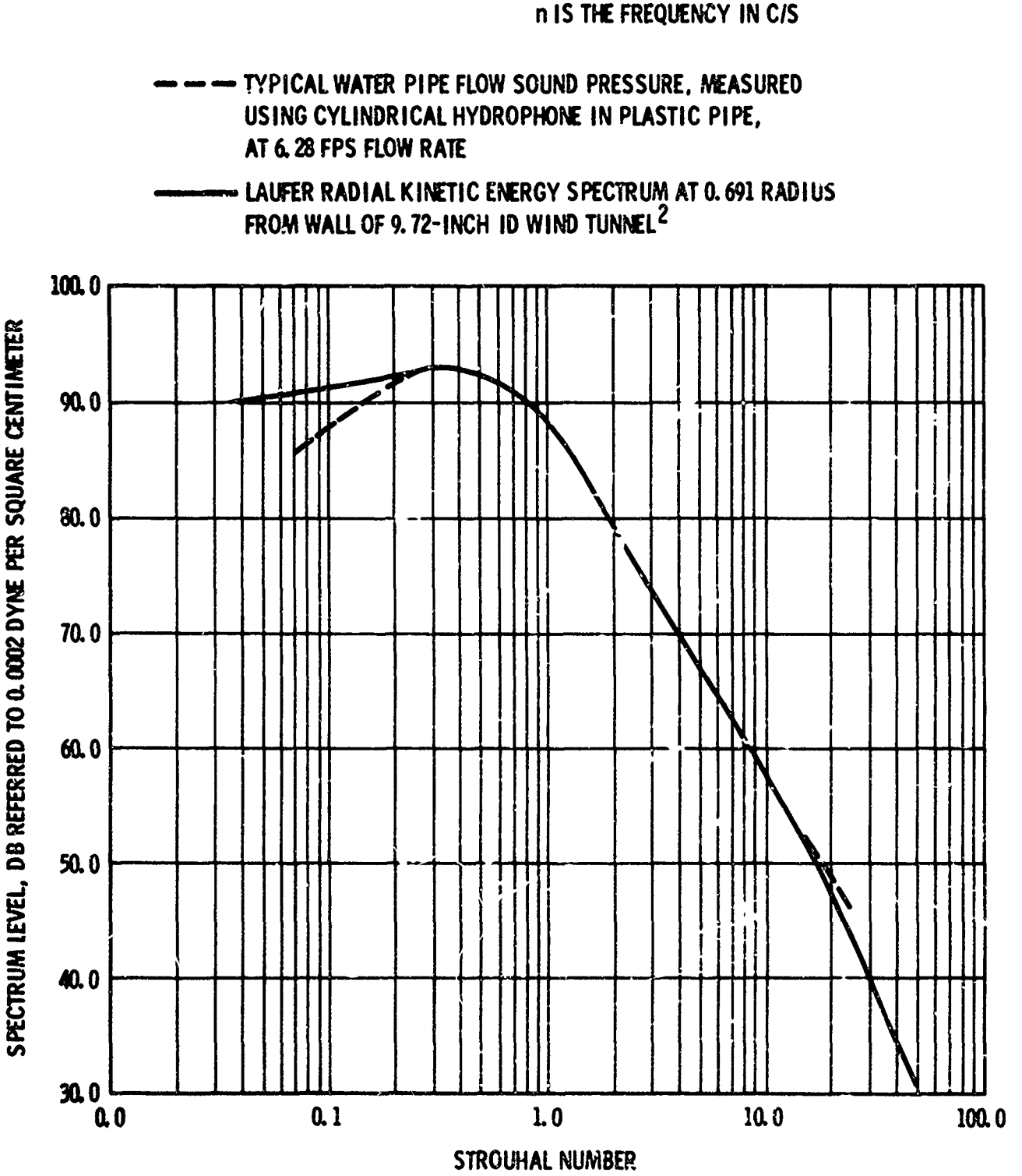

Figure 13. Comparison of Laufer's kinetic energy spectrum with pressure spectrum of water pipe flow measurements.

BROADBAND MAGNITUDES

Broadband amplitude values were obtained directly from rectified rms analog tracings, and from numerical integration of spectra levels and numerical analysis of Polaroid photos. The Sanborn traces of hydrophone and micrometer signal levels were compared to parallel traces of the reference oscillator and white-noise generator signal levels.

In figures 14 and 15, ratios of broadband magnitudes, measured from both types of hydrophones, to measured dynamic pressure head, p/q, are plotted against Reynolds number. Theoretical p/q values, based on the equation $p/q = k^2F$ (where F is Blasius' relationship between the friction coefficient and the Reynolds number equal to $0.079/R^{.25}$), with k equal to values of 0.9, 1.0, and 1.44, are shown as straight lines. The value of k is the ratio of the fluctuating radial stress to the wall shear stress in the constant stress layer (it is assumed that the fluctuating radial pressure at the pipe wall may be nearly equal in magnitude to the fluctuating pressure in the constant stress layer). The measured k value, with the hydrophone mounted flush with the inside of the pipe wall and responding only to radial pressure components, can be expected to be 0.9. With a hydrophone responding to the mean of the fluctuating components, the k value should be 1.44.

Effective broadband magnitudes measured by hydrophones are shown in figures 16 and 17, plotted against measured dynamic pressure head, $q = \frac{1}{2}\rho\overline{u}^2$, where ρ is the fluid density and $\overline{u}$ is the mean fluid velocity.

NOTE:

1. POINTS PLOTTED REPRESENT VALUES OF p/q COMPUTED FROM MEASURED DATA.
2. STRAIGHT-LINE CURVES FOR VALUES OF k SHOW THEORETICAL p/q PLOTS BASED UPON THE EQUATION $p/q = k^2F$ WHERE F IS BLASIUS' RELATIONSHIP BETWEEN THE FRICTION COEFFICIENT f AND THE REYNOLDS NUMBER; $F = 0.079/R^{.25}$. k IS THE VELOCITY RATIO OF FLUCTUATING RADIAL STRESS TO THE WALL SHEAR STRESS IN THE CONSTANT STRESS LAYER.

p IS THE MEASURED RMS BROADBAND VALUE

$q = 1/2 \rho \bar{u}^2$

REYNOLDS NUMBER, $R = \bar{u}D\rho/\mu$

WHERE ρ IS THE FLUID DENSITY

$\bar{u}$ IS THE MEAN, AVERAGE FLUID VELOCITY

D IS THE PIPE INSIDE DIAMETER

μ IS THE FLUID DYNAMIC VISCOSITY

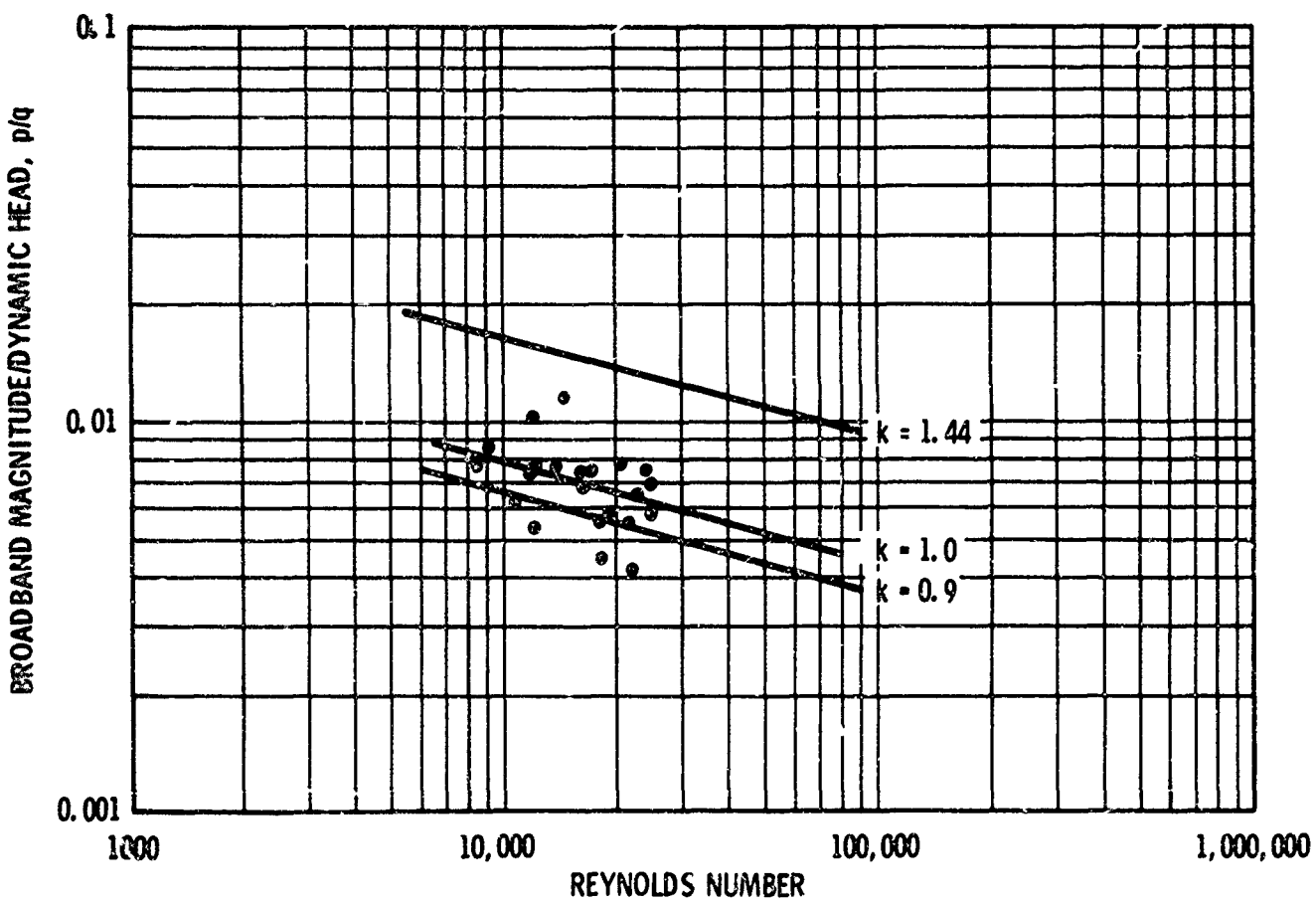

Figure 14. Bimorph hydrophone broadband magnitude to dynamic head ratios, plotted against Reynolds number.

NOTE:

1. POINTS PLOTTED REPRESENT VALUES OF p/q COMPUTED FROM MEASURED DATA.
2. STRAIGHT-LINE CURVES FOR VALUES OF k SHOW THEORETICAL p/q PLOTS BASED UPON THE EQUATION $p/q = k^2F$ WHERE F IS BLASIUS' RELATIONSHIP BETWEEN THE FRICTION COEFFICIENT f AND THE REYNOLDS NUMBER; $F = 0.079/R^{.25}$. k IS THE VELOCITY RATIO OF FLUCTUATING RADIAL STRESS TO THE WALL SHEAR STRESS IN THE CONSTANT STRESS LAYER.

p IS THE MEASURED RMS BROADBAND VALUE

$q = 1/2\rho\bar{u}^2$

REYNOLDS NUMBER, $R = \bar{u}D\rho/\mu$

WHERE ρ IS THE FLUID DENSITY

$\bar{u}$ IS THE MEAN, AVERAGE FLUID VELOCITY

D IS THE PIPE INSIDE DIAMETER

μ IS THE FLUID DYNAMIC VISCOSITY

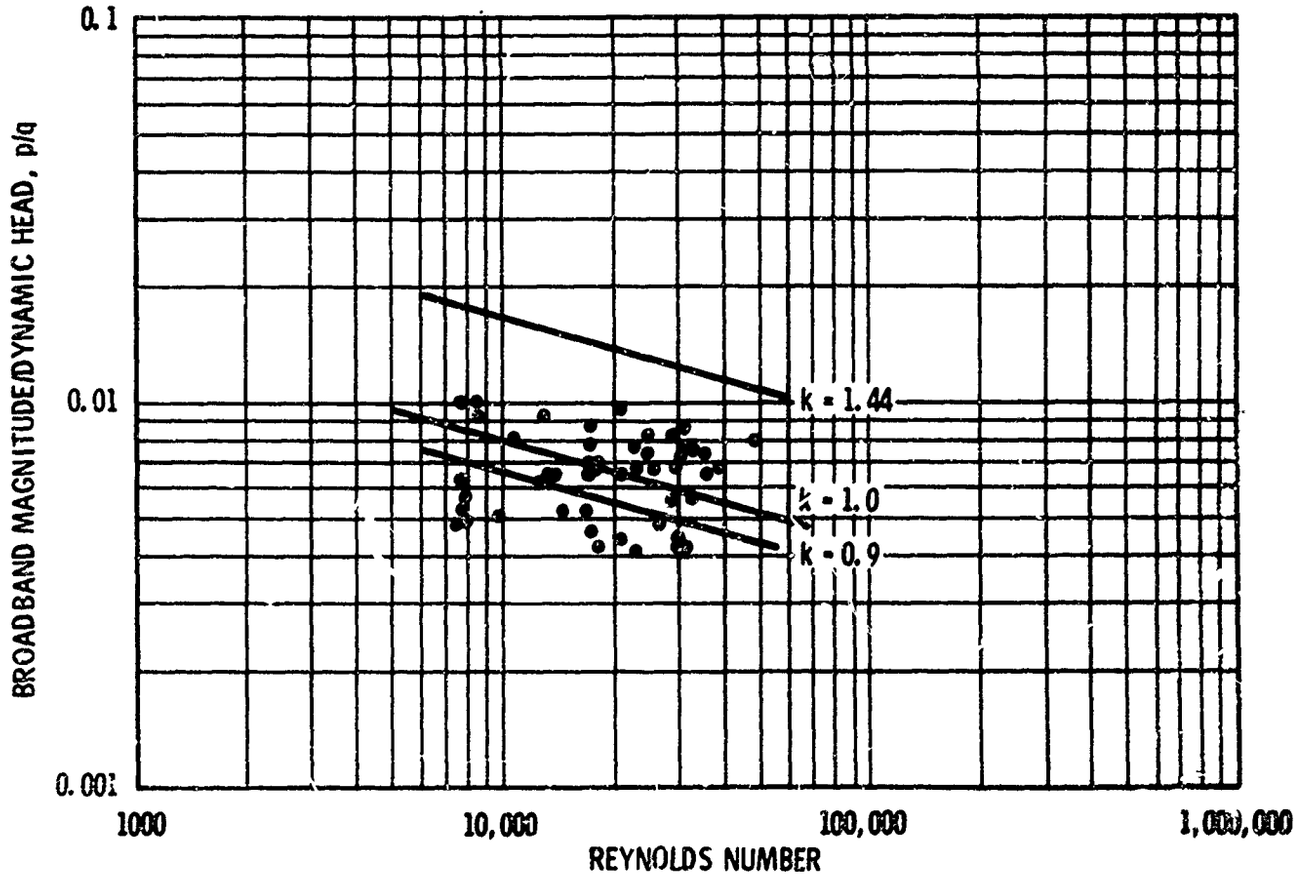

Figure 15. Cylindrical hydrophone broadband magnitude to dynamic head ratios, plotted against Reynolds number.

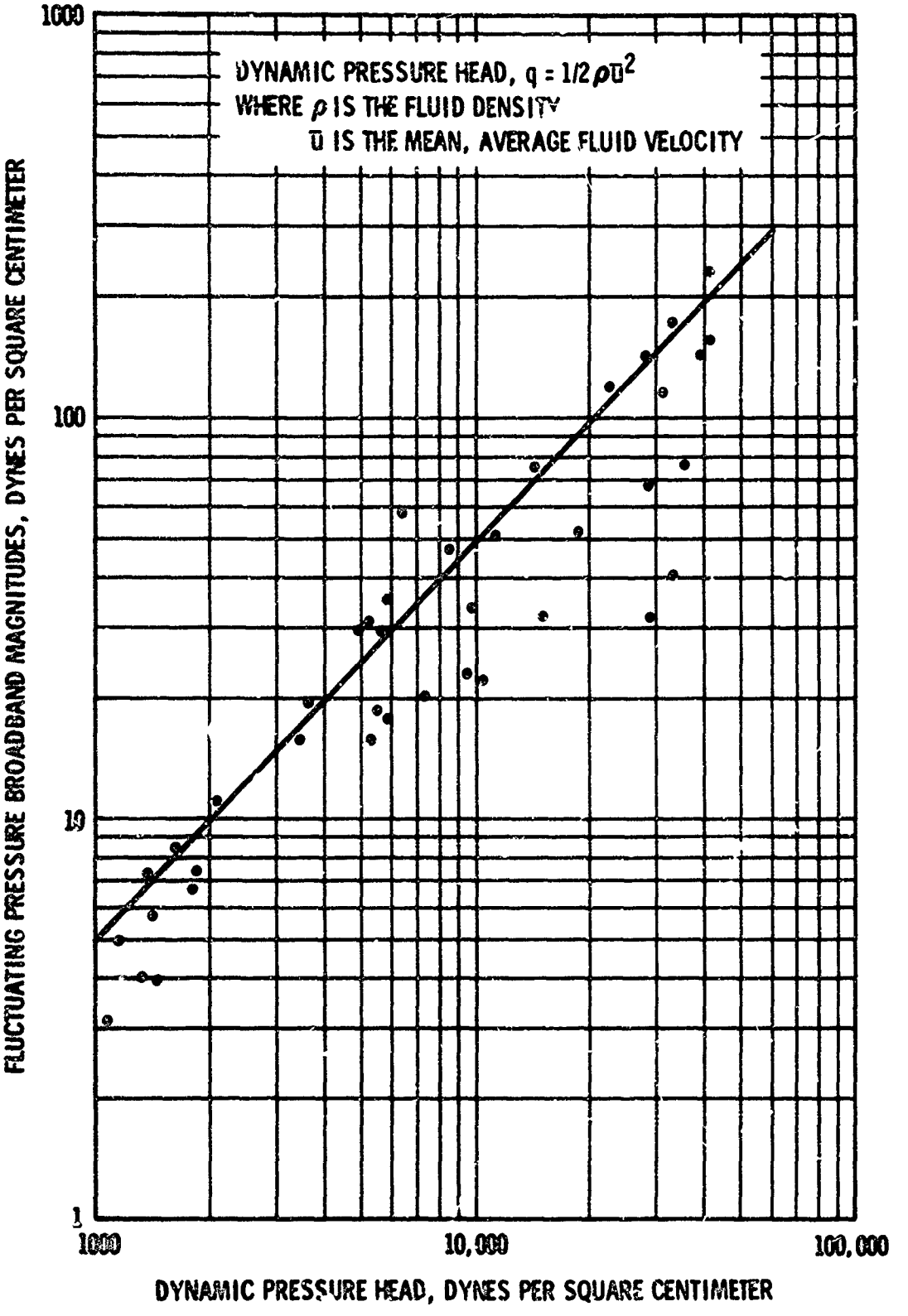

Figure 16. Cylindrical hydrophone broadband magnitudes of fluctuating pressure at wall of brass pipe, plotted against dynamic pressure.

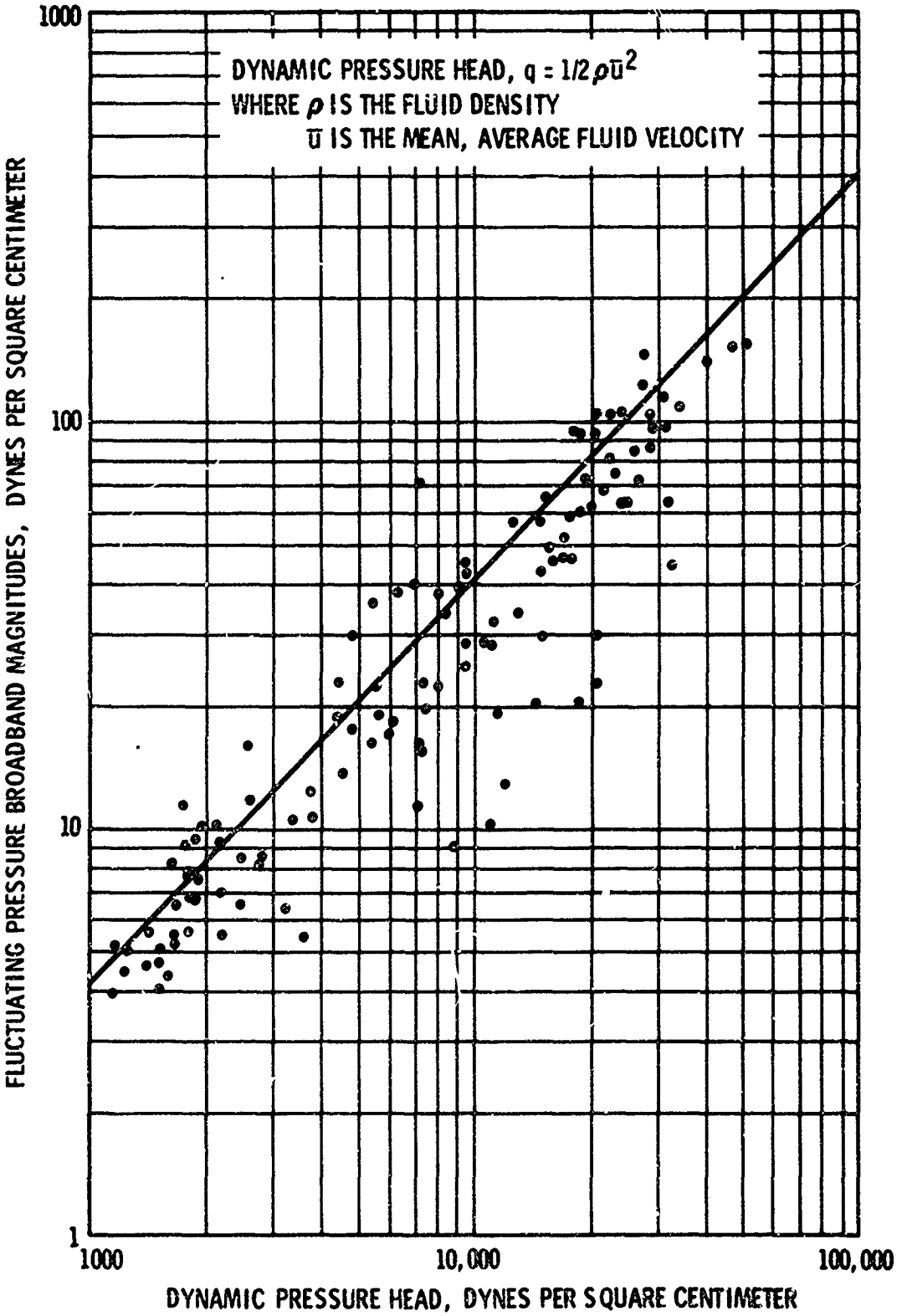

Figure 17. Measured effective hydrophone broadband magnitudes of pipe wall fluctuating pressure, plotted against dynamic pressure.

WALL SHEAR STRESS/DYNAMIC HEAD RATIO

The wall shear stress/dynamic head dimensionless ratio can be used to evaluate the fluctuating pressure to dynamic head ratio, p/q. The wall stress/inertia head ratio, τ/q, is nearly constant over the range of water pipe flow experiments, but is a function of the Reynolds number. Wall shear values were measured with a differential-pressure manometer over lengths of test pipe during the water flow experiments, and were recorded on data sheets. Figures 18 and 19 show the wall shear stress/dynamic head ratio plotted against dynamic head and against Reynolds number. The variation with Reynolds number resembles the Blasius friction equation discussed under theory in Appendix B.

PIPE WALL DISPLACEMENT

The mutual inductance micrometer obtained measurable fluctuations from plastic and brass pipe after the pipe wall thickness was reduced to 0.003 inch near the probe: measurable displacement was dependent upon wall thickness. Radial displacement above quiescence of plastic pipe with 0.003-inch thick wall is shown plotted against broadband wall pressure in figure 20. Power spectra for radial displacement of plastic and brass walls are shown in figures 11 and 12, plotted against frequency.

WALL SHEAR STRESS, $\tau = \Delta P r / L 2$
WHERE ΔP IS THE PRESSURE DROP OVER THE LENGTH L
r IS THE PIPE RADIUS
L IS THE LENGTH OVER WHICH ΔP WAS MEASURED
DYNAMIC PRESSURE HEAD, $q = 1/2 \rho \bar{u}^2$
WHERE ρ IS THE FLUID DENSITY
$\bar{u}$ IS THE MEAN, AVERAGE FLOW VELOCITY

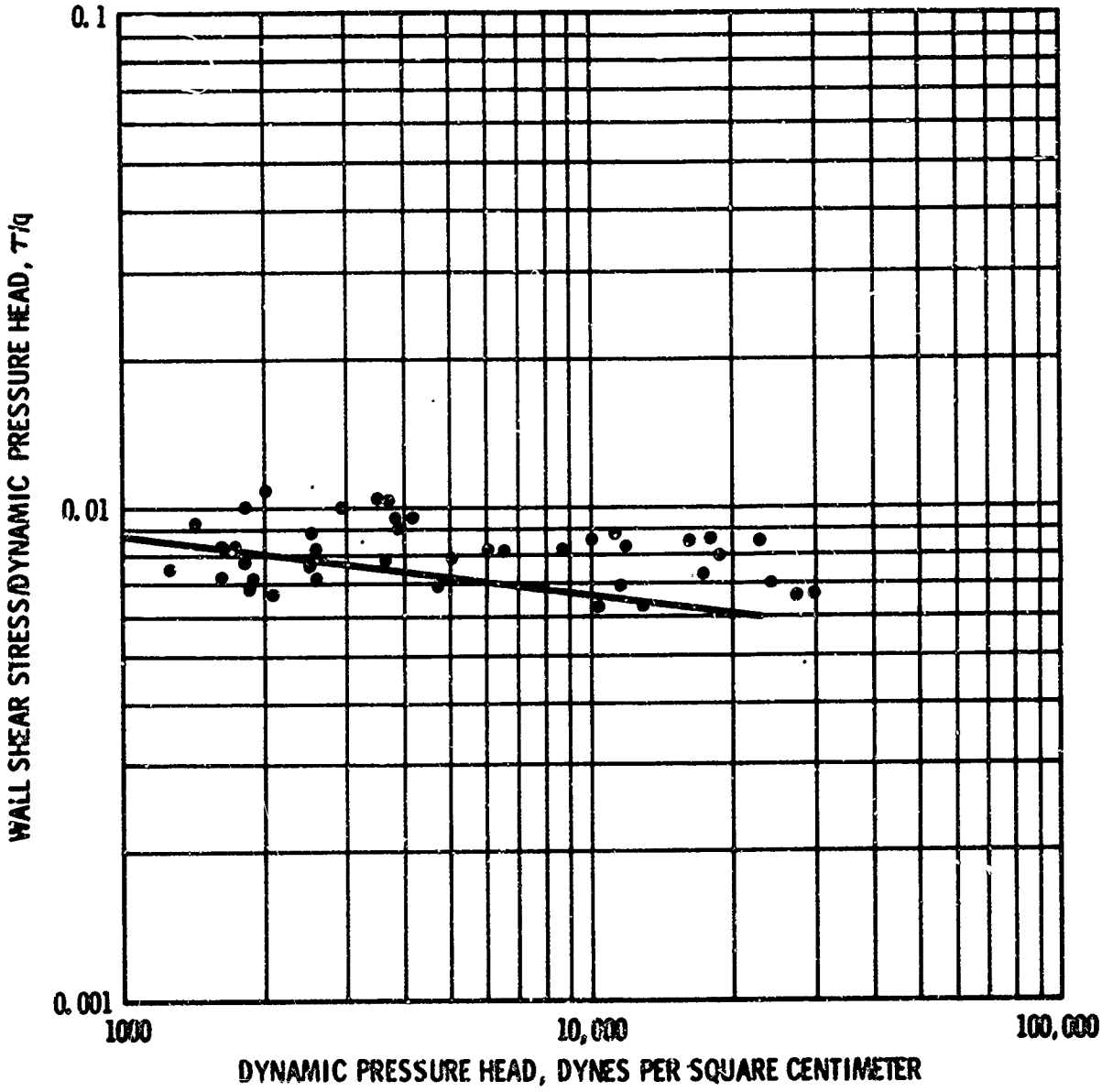

Figure 18. Wall shear stress to dynamic pressure ratios, plotted against dynamic pressure head.

WALL SHEAR STRESS, $\tau = \Delta P r/L2$
WHERE ΔP IS THE PRESSURE DROP OVER LENGTH L
r IS THE PIPE RADIUS
L IS THE LENGTH OVER WHICH ΔP WAS MEASURED
DYNAMIC PRESSURE HEAD, $q = 1/2 \rho \bar{u}^2$, AND
REYNOLDS NUMBER, $R = \bar{u} D \rho / \mu$,
WHERE ρ IS THE FLUID DENSITY
$\bar{u}$ IS THE MEAN, AVERAGE FLUID VELOCITY
D IS THE PIPE INSIDE DIAMETER
μ IS THE FLUID DYNAMIC VISCOSITY

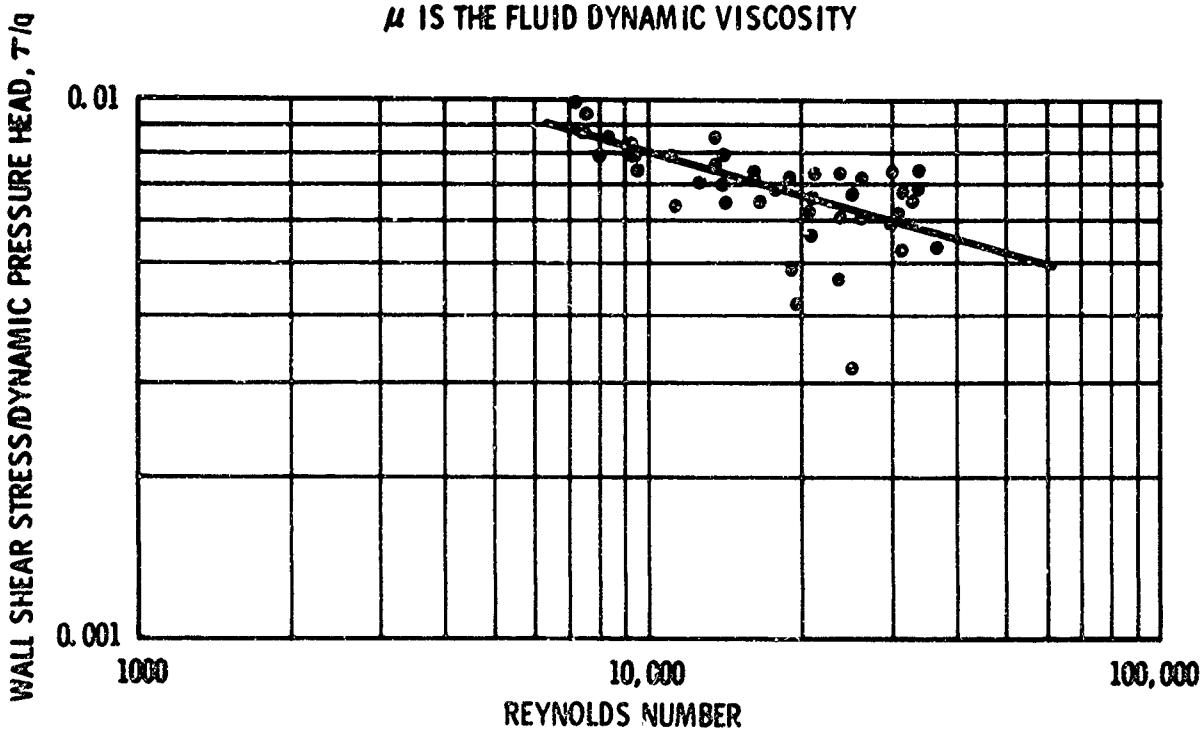

Figure 19. Wall shear stress to dynamic pressure head ratios, plotted against Reynolds number.

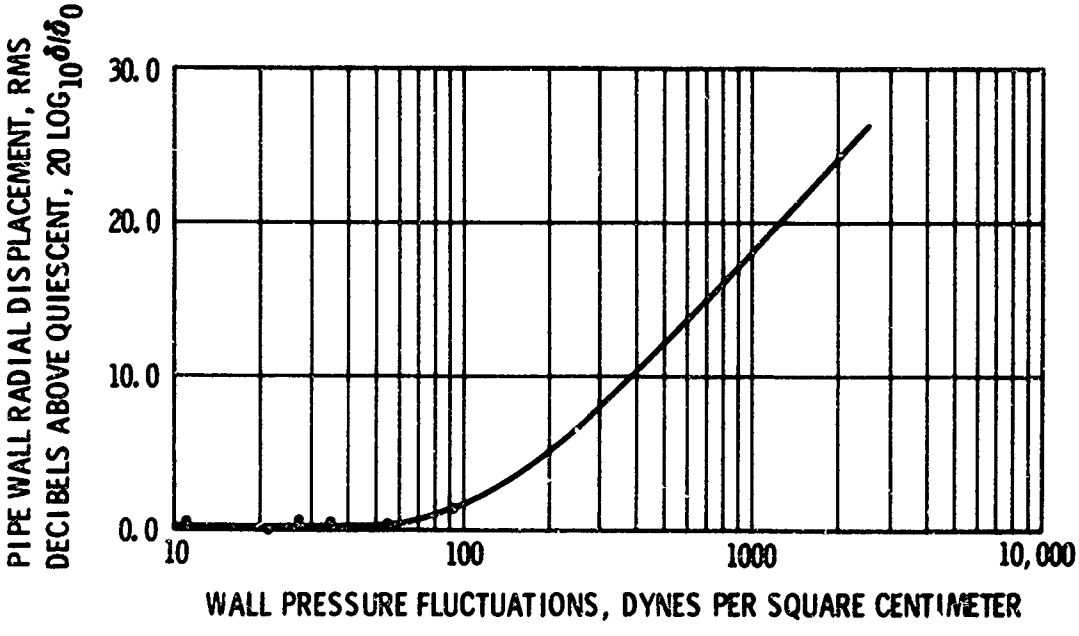

Figure 20. Micrometer measurements of 0.003-inch-thick plastic pipe wall displacement, plotted against broadband wall pressure fluctuations measured with cylindrical hydrophone.

CONCLUSIONS AND RECOMMENDATIONS

This study of water noise in pipes has demonstrated the feasibility and economy of "water tunnel" experimentation in turbulent flow noise research. The study also demonstrated the applicability of the theory of classical mechanics to water flow, and enabled the derivation of an engineering method for computing values of water flow noise for given conditions.

Conduct of water flow noise research under laboratory conditions enables control of the variables which is possible in no other way. This basic research establishes criteria applicable to further laboratory studies, research under more severe conditions, and to developmental programs.

The "water tunnel" type of experimentation should be continued to study higher flow rates and response frequencies. Application of the results of this study to design and development of components and systems for research and service use should be encouraged.

REFERENCES

1. Navy Electronics Laboratory Report 1182, Flow Noise of Streamlined Bodies Falling Freely in Water, by P. O. Laitinen, 19 September 1963

2. National Advisory Committee for Aeronautics Report 1174, The Structure of Turbulence in Fully Developed Pipe Flow, by J. Laufer, 1954

3. National Advisory Committee for Aeronautics Report 1247, Characteristics of Turbulence in a Boundary Layer With Zero Pressure Gradient, by P. S. Klebanoff, 1955

4. Schubauer, G. B., "Turbulent Processes as Observed in Boundary Layer and Pipe," Journal of Applied Physics, v. 25, p. 188-196, February 1954

5. Townsend, A. A., The Structure of Turbulent Shear Flow, Cambridge University Press, 1956

6. Hinze, J. A., Turbulence, McGraw-Hill, 1959

7. Willmarth, W. W., "Wall Pressure Fluctuations in a Turbulent Boundary Layer," Acoustical Society of America. Journal, v. 28, p. 1048-1053, November 1956

8. Nikuradse, J., "Turbulente Strömungen in nicht Kreisförmigen Röhren," Ingenieur-Archiv, v. 1, p. 306, 1930

9. Blasius, H., "Das Ähnlichkeitsgesetz bei Reibungsvorgängen in Flüssigkeiten," Mitteilungen über Forschungsarbeiten auf dem Gebiete des Ingenieurwesens, No. 131, 1913

10. Lighthill, M. J., "On Sound Generated Aerodynamically, I: General Theory," Royal Society of London. Proceedings. Series A: Mathematical and Physical Sciences, v. 211, p. 564-587, 20 March 1952

References (Continued)

11. Lighthill, M. J., "On Sound Generated Aerodynamically, II: Turbulence as a Source of Sound," Royal Society of London. Proceedings. Series A: Mathematical and Physical Sciences, v. 222, p. 1-32, 23 February 1954

12. Proudman, I., "The Generation of Noise by Isotropic Turbulence," Royal Society of London. Proceedings. Series A: Mathematical and Physical Sciences, v. 214, p. 119-132, 7 August 1952

13. de Kármán, T. and Howarth, L., "On the Statistical Theory of Isotropic Turbulence," Royal Society of London. Proceedings. Series A: Mathematical and Physical Sciences, v. 164, p. 192-215, 21 January 1938

14. Taylor, G. I., "Statistical Theory of Turbulence," Royal Society of London. Proceedings. Series A: Mathematical and Physical Sciences, v. 151, p. 421-478, 2 September 1935

15. Taylor, G. I., "The Spectrum of Turbulence," Royal Society of London. Proceedings. Series A: Mathematical and Physical Sciences, v. 164, p. 476-490, 18 February 1938

16. David Taylor Model Basin Report 1260, Pressure Fluctuations on the Wall Adjacent to a Turbulent Boundary Layer, by M. Harrison, December 1958

17. Underwater Sound Laboratory Report 559, Wall Pressure Correlations in Turbulent Pipe Flow, by H. P. Blakewell and others, 20 August 1962

SUPPLEMENTAL BIBLIOGRAPHY

Lee, Y. W. and others, "Application of Correlation Analysis to the Detection of Periodic Signals in Noise," Institute of Radio Engineers, Proceedings, v. 38, p. 1165-1171, October 1950

Bartlett, M. S., "Periodogram Analysis and Continuous Spectra," Biometrika, v. 37, p. 1-16, June 1950

Lee, Y. W., Statistical Theory of Communication, Wiley, 1960

Schlichting, H., Boundary Layer Theory, 4th ed., McGraw-Hill, 1960

DISCLAIMER NOTICE

THIS DOCUMENT IS BEST QUALITY PRACTICABLE. THE COPY FURNISHED TO DTIC CONTAINED A SIGNIFICANT NUMBER OF PAGES WHICH DO NOT REPRODUCE LEGIBLY.

OR are
Blank pgs
that have
Been Removed

BEST AVAILABLE COPY

APPENDIX A: EXPERIMENTAL HYDROPHONES

Since hydrophone responsiveness depends upon size, material, shape, and polarity of the element, the accuracy of the measured data depends upon accurate hydrophone calibration.

The cantilever-bimorph type shown in figure A-1 would not be expected to respond equally over its face if it were calibrated by a plane wave; its best response area is near its free edge, and its effective length may be less than half its true length. The bimorph type experimental hydrophones were calibrated in a free field and also within a test pipe section, using a small probe reference hydrophone. Calibration results are shown in figure A-2; the response measured within the pipe is several decibels higher than that measured in a free field.

The radially polarized barium titanate cylindrical type hydrophone, figure A-3, resembles those used in service applications. This type was calibrated by plane waves, with results as shown in figures A-4 through A-7. Its response to wall pressure fluctuations can be expected to be similar to the sum of the signals from the elemental areas, added statistically.

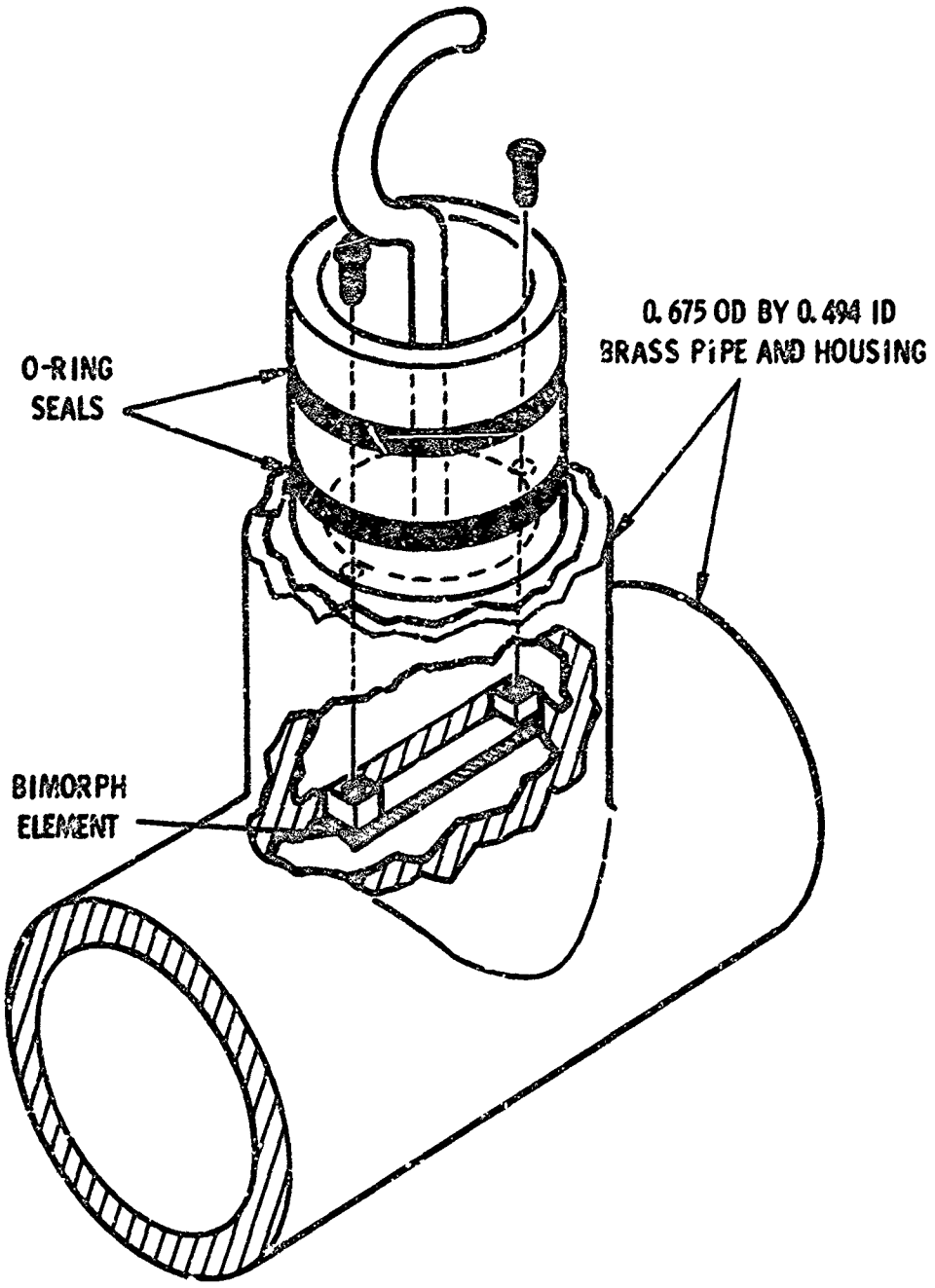

Figure A-1. Barium zirconium titanate bimorph hydrophone with element mounted in machined slot, flush with pipe inside wall.

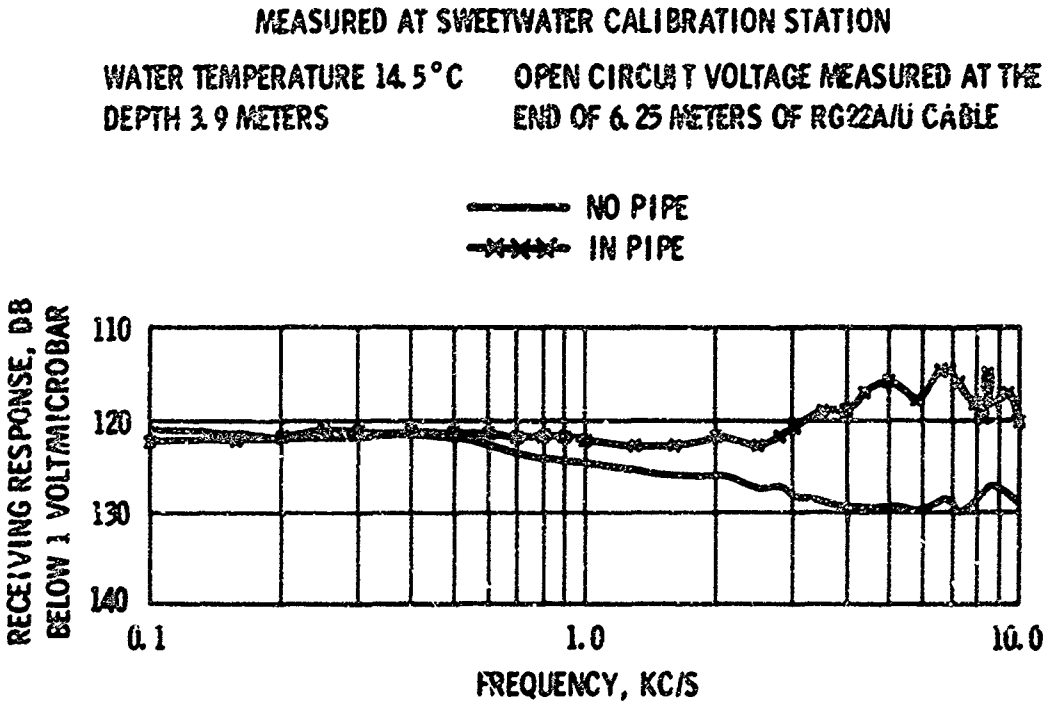

Figure A-2. Bimorph hydrophone receiving response calibration in a free field and inside a pipe.

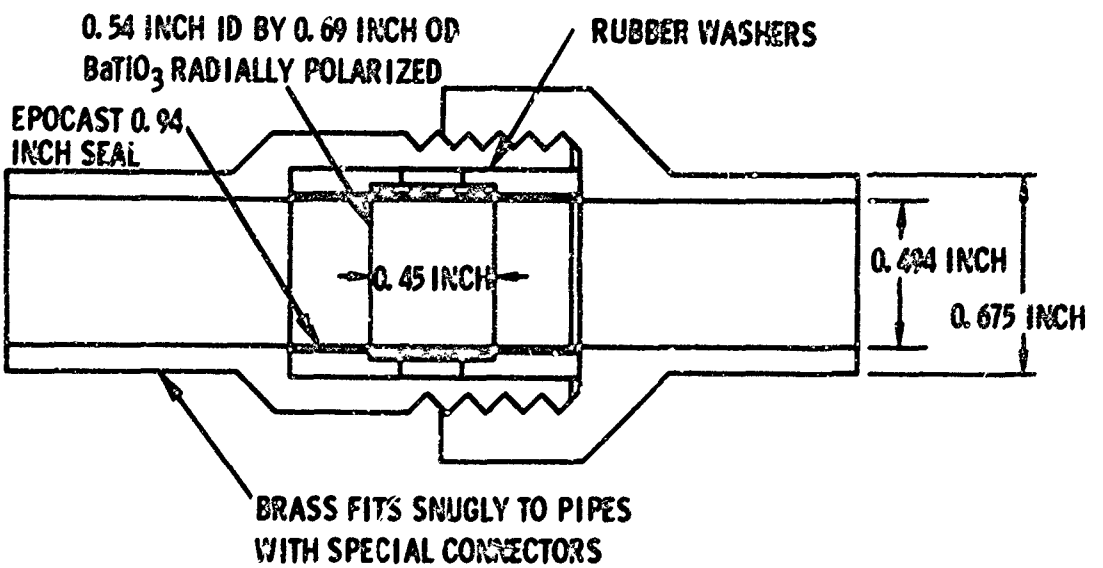

Figure A-3. Radially polarized barium titanate cylindrical hydrophone.

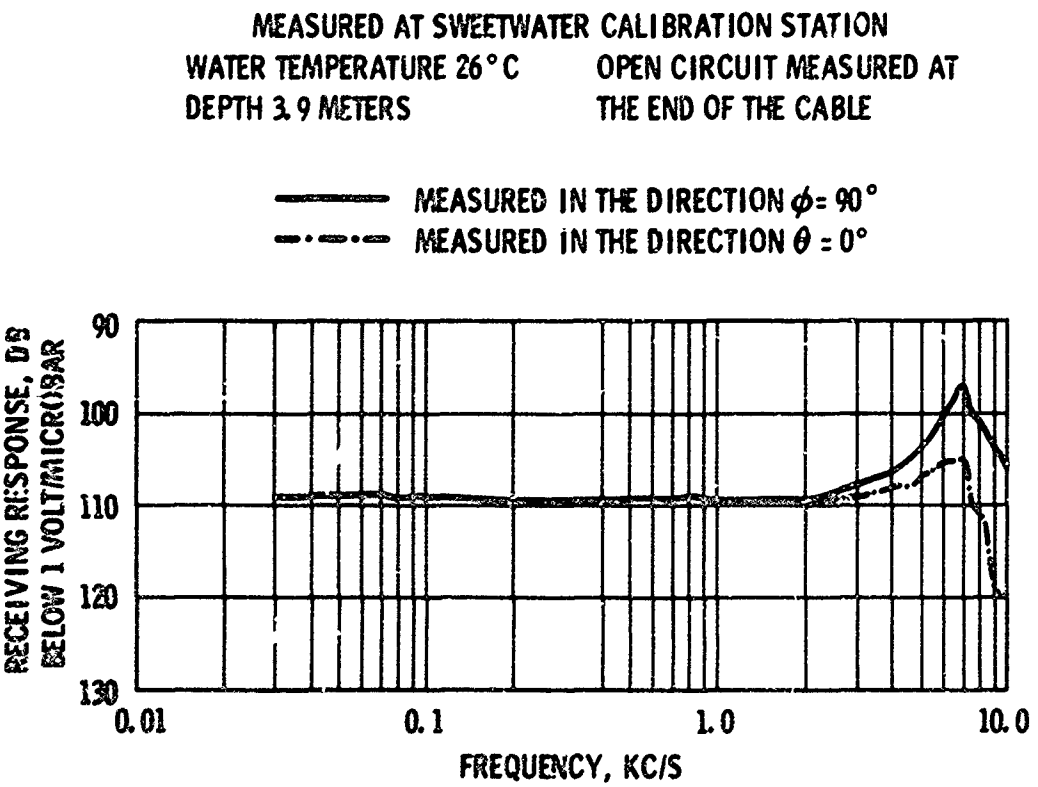

Figure A-4. Cylindrical hydrophone receiving response calibration.

SWEETWATER CALIBRATION STATION — 3 AUGUST 1959
$\theta = 0°$
WATER TEMPERATURE 26°C — TEST DISTANCE 2 METERS
DEPTH 3.9 METERS — $\phi = 90°$
SCALE 10 DB PER RADIAL DIVISION — ROTATE θ

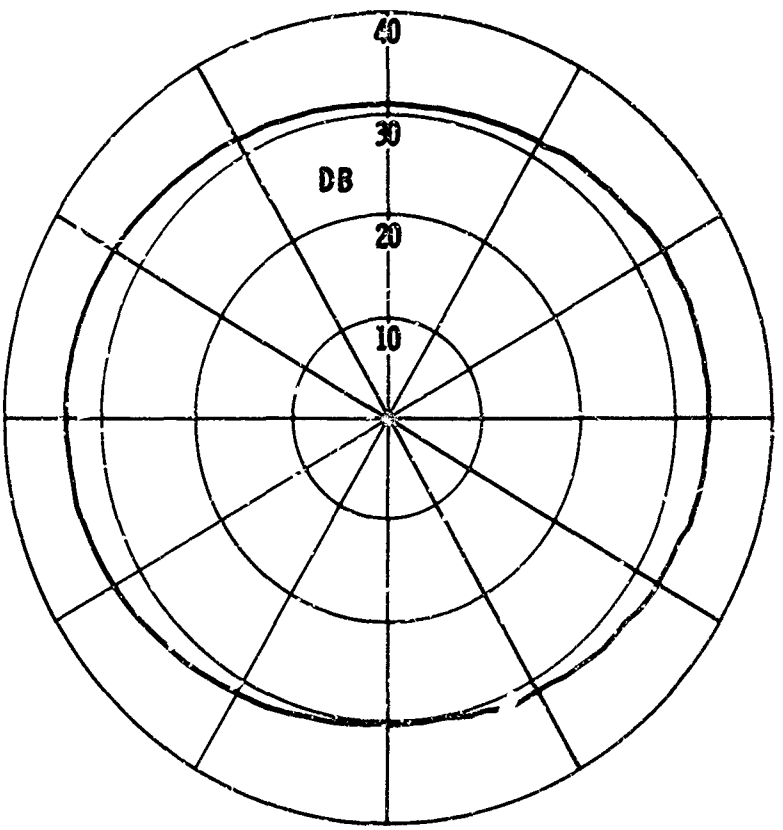

Figure A-5. Cylindrical hydrophone calibration directivity pattern, 5 kc/s.

SWEETWATER CALIBRATION STATION
$\theta = 0°$

3 AUGUST 1959

WATER TEMPERATURE 26°C
DEPTH 3.9 METERS
SCALE 10 DB PER RADIAL DIVISION

TEST DISTANCE 2 METERS
$\phi = 90°$
ROTATE θ

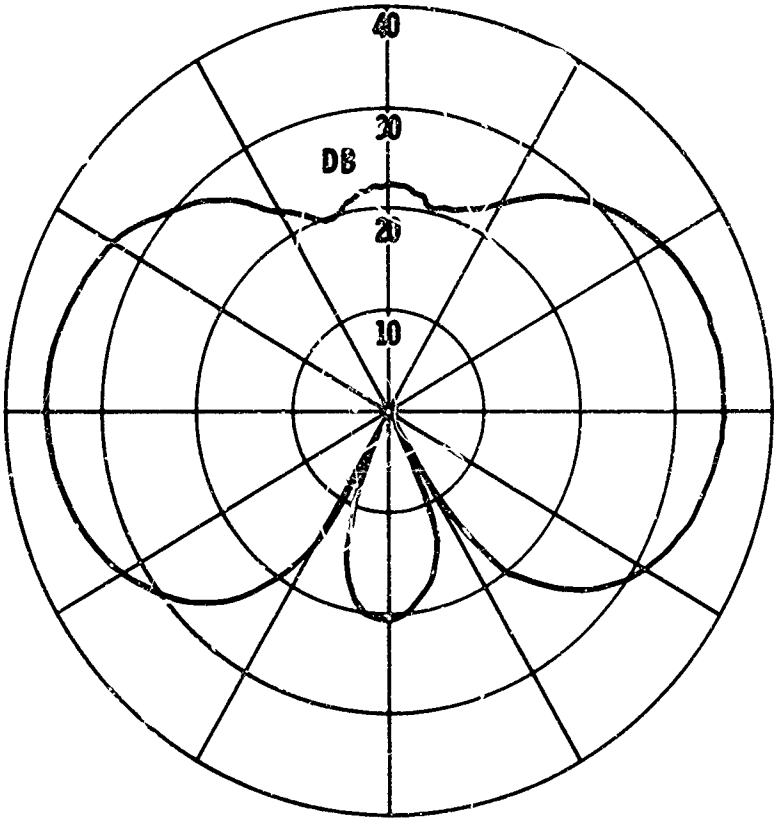

Figure A-6. Cylindrical hydrophone calibration directivity pattern, 10 kc/s.

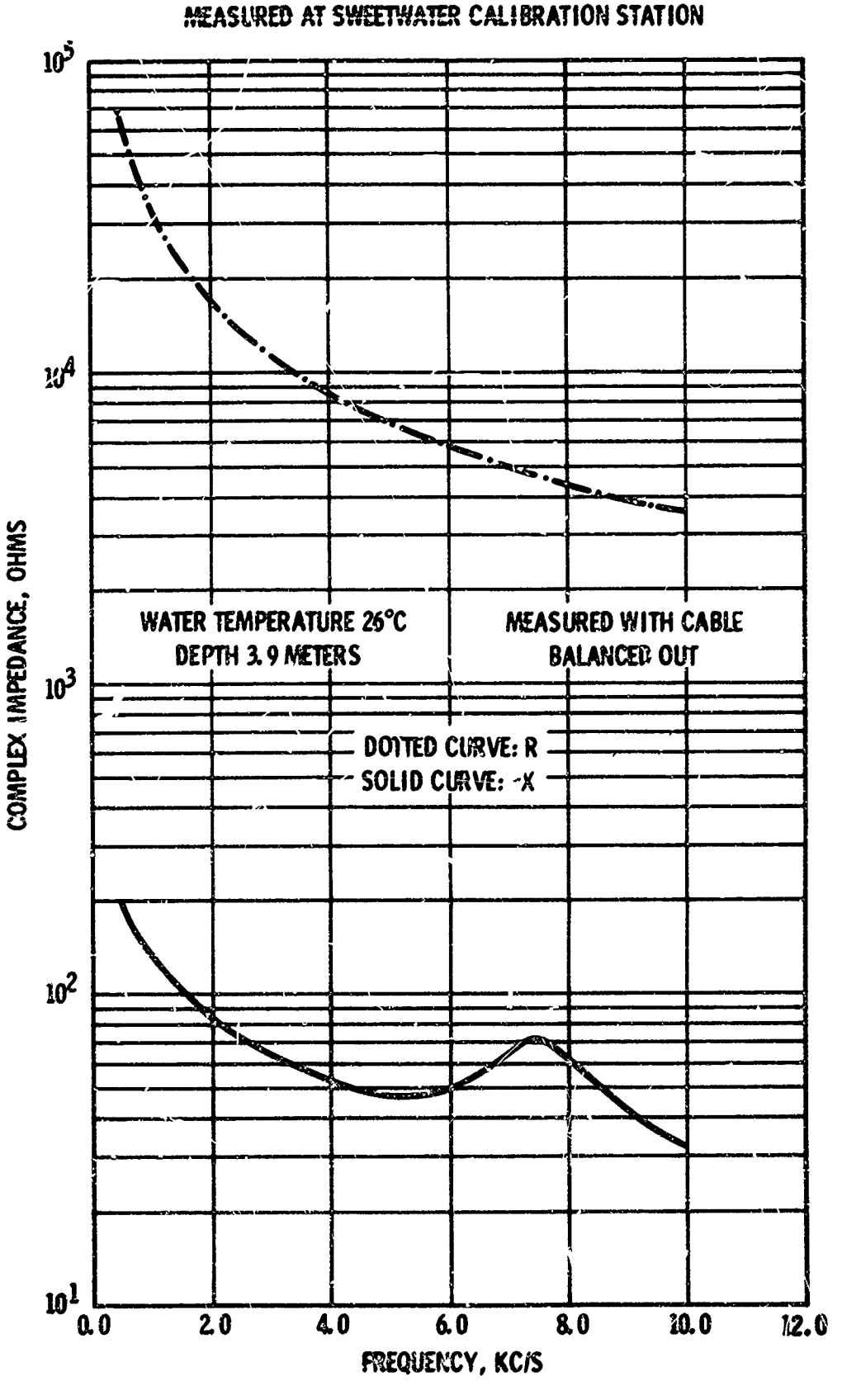

Figure A-7. Cylindrical hydrophone complex impedance calibration, series measurement.

REVERSE SIDE BLANK

DISCLAIMER NOTICE

THIS DOCUMENT IS BEST QUALITY PRACTICABLE. THE COPY FURNISHED TO DTIC CONTAINED A SIGNIFICANT NUMBER OF PAGES WHICH DO NOT REPRODUCE LEGIBLY.

OR are
Blank pgs
that have
Been Removed

BEST AVAILABLE COPY

APPENDIX B: THEORY

MECHANICS OF FLOW

The flow of water through a pipe can be explained by classical mechanics. The behavior of a continuous medium (which the water is assumed to be) under mechanical and thermal environmental influences is controlled by the laws of conservation of mass, conservation of energy, and non-decreasing entropy, and by Newton's second law of motion in the form used in fluid mechanics under the name of the Navier Stokes equations. The first law is the equation of continuity. The next two are the first and second laws of thermodynamics. The thermodynamic and the mechanical behavior are coupled through the equation for the conservation of energy, and through the equation of state which relates stress with strain. The thermal and mechanical problems can be separated when the rise in temperature and the volume changes are small. The cross-coupling by compressibility is usually small for a nearly incompressible fluid like water. For the pipe flow experiments, the thermal and mechanical problems can be separated. Only the mechanical problem is investigated at length herein.

Energy is required to push the water through the pipe. Friction opposes the motion, and the water does not slip freely at the pipe wall. Part of the friction energy appears as the pressure energy of flow noise, with most of the energy eventually converted to heat. If the water could slide through the pipe without losses, it would be called an ideal fluid. An ideal fluid does not have dissipation and cannot support shearing stresses in motion. All moving real fluids show dissipation which appears entirely as shear energy, since there can be no permanent volume changes in real fluids. The most common theoretical fluid considered is the Newtonian fluid in which all the dissipation is expressible in terms of strain rates alone. This fluid is defined by a simple relationship (below) between the shear stresses and strain rates through the fluid-characteristic coefficient called the viscosity, which determines the dissipation:

$$\tau_{ij} = 2\mu\dot{\nu}_{ij} = \mu\left(\frac{\partial u_i}{\partial x_j} + \frac{\partial u_j}{\partial x_i}\right) \tag{1}$$

where τ_{ij} is the shearing stress, with $i \neq j$

μ is the coefficient of viscosity

u_i, u_j are the velocity components

$\dot{\nu}_{ij}$ is the strain rate in shear, with $i \neq j$

x_i, x_j are the space distances.

In a moving fluid, the stress depends on both the static strains and the strain rates. In an isotropic elastic solid, the equation of state shows that the stress is related to the strains through two elastic constants. For a fluid that is not moving, mean stresses are related to mean strains through one elastic constant:

$$,\sigma = B(\Delta - \alpha T) = B(3\,,\epsilon - \alpha T) \tag{2}$$

where $,\sigma$ is the mean stress

$,\epsilon$ is the mean strain, equal to $\Delta/3$

B is the bulk modulus of elasticity

Δ is the dilation, or volume change per unit volume

α is the coefficient of volume expansion

T is the temperature.

Static fluids cannot support shearing stresses. The state of stress for a moving fluid is the sum of the mean stress, or hydrostatic pressure, and that resulting from the fluid motion. Because of viscosity, the moving fluid also has shear stresses that are proportional to strain rates. The stress in a moving fluid is given by the formula:

$$\sigma_{ij} = \mu\left(\frac{\partial u_i}{\partial x_j} + \frac{\partial u_j}{\partial x_i} - \frac{2}{3}\frac{\partial u_k}{\partial x_k}\right)\delta_{ij} - P\delta_{ij} \tag{3}$$

where σ_{ij} is the stress

δ_{ij} is the Kronecker delta (equal to 1 when $i=j$ and zero when $i \neq j$)

μ is the viscosity

P is the hydrostatic pressure

u_i, u_j are the velocities

x_i, x_j are space dimensions

u_k is free Kronecker index for velocity

x_k is free Kronecker index for distance.

The energy dissipation per unit volume in a Newtonian fluid due to mechanical causes is given by:

$$\psi = \sigma_{ij}\dot{\nu}_{ij} = 2\mu(\dot{\nu}_{ij})^2 \tag{4}$$

where ψ is the energy dissipation per unit volume

σ_{ij} is the stress

$\dot{\nu}_{ij}$ is the strain rate in shear ($i \neq j$)

μ is the viscosity.

The problem of the viscous fluid is stated in the following equations:

Continuity:

$$\frac{\partial \rho}{\partial t} + \frac{\partial (\rho u_k)}{\partial x_k} = 0 \tag{5}$$

where ρ is the fluid density

u_k is free Kronecker index for velocity

x_k is free Kronecker index for distance.

The First Law of Thermodynamics:

$$\rho\frac{dh}{dt} = \rho\frac{dT}{dt} - \rho T\frac{ds}{dt} \qquad \mu\frac{de}{dt} + \rho\frac{d\Delta}{dt} = -\frac{\partial q_i}{\partial x_i} + 2\mu(\dot{\nu}_{ij})^2 \tag{6}$$

where h is the enthalpy per unit mass

s is the entropy per unit mass

t is time

T is the temperature in degrees absolute

e is the internal energy per unit mass

Δ is the dilation

ρ is the fluid density

q_i is the heat conducted per unit volume

μ is the viscosity

$\dot{\nu}_{ij}$ is the strain rate

C is the specific heat

x_i is the distance.

The Second Law of Thermodynamics:

$$\rho ds + \frac{\partial}{\partial x_i}\left(\frac{q_i}{T}\right) \geq 0 \tag{7}$$

where s is the entropy per unit mass

x_i is the distance

q_i is the heat conducted per unit volume

T is the temperature.

Newton's Second Law of Motion:

$$\rho F_i + \frac{\partial \sigma_{ij}}{\partial x_j} = \rho \frac{du_i}{dt} \tag{8}$$

where F_i is the external force per unit mass

σ_{ij} is the stress

x_j is the distance

u_i is the velocity

t is time.

The First Law is the energy relation for the motion. It can be used to develop the equations for the thermal boundary layer using Fourier's law of heat conduction (which equates heat conducted in a direction to the product of the space derivative of temperature in that direction) and the constant of conductivity. The Second Law of Thermodynamics states that the net change in entropy in a region (the entropy generated in the region and conducted out of the region) must be zero or greater. Substitution of the complete stress-strain relationship, equation 3, into the Second Law of Motion leads to the fundamental equation of fluid mechanics, the Navier Stokes equation:

$$\rho \frac{du}{dt} = \rho F_i + \mu \frac{\partial^2 u_k}{\partial x_k^2} + \frac{\mu}{3} \frac{\partial}{\partial x_i} \left(\frac{\partial u_k}{\partial x_k} \right) - \frac{\partial p}{\partial x_i} \tag{9}$$

where ρ is the fluid density

u is a velocity component

t is time

F_i is the external force per unit mass

μ is the coefficient of viscosity

u_k is free Kronecker index for velocity

x_k is free Kronecker index for distance

x_l is the distance.

SIMILARITY CONDITIONS OF TURBULENCE

O. Reynolds made a detailed study of the character of flow in 1883. Many of the concepts of turbulence are due to Reynolds who noted that for similar flows about geometrically similar bodies with different fluids, different velocities, and different densities, the forces on the fluid particles must bear a fixed ratio. When various measurable quantities and dimensional constants are completely related, an equation can be written in terms of dimensionless ratios to describe the relationship. In order for two flows to be similar, the ratios must be the same for the flows. For similar flow processes, the dimensionless ratios are the ratios between the various types of forces. The principal ratios are listed below:

$$\frac{\text{inertia}}{\text{viscous}} = \frac{\rho V l}{\mu} \qquad \text{Reynolds number}$$

$$\frac{\text{pressure}}{\text{viscous}} = \frac{P}{\tau} \qquad \text{pressure/shear stress}$$

$$\frac{\text{pressure}}{\text{elastic}} = \frac{p}{B} = \frac{p}{\rho c^2} \qquad \text{pressure/acoustic}$$

$$\frac{\text{pressure}}{\text{inertia}} = \frac{p}{\rho V^2} \qquad \text{pressure/dynamic head}$$

$$\frac{\text{inertia}}{\text{elastic}} = \frac{\rho V^2}{B} = \frac{V^2}{c^2} \qquad \text{Mach number}$$

$$\frac{\text{inertia}}{\text{gravity}} = \frac{V^2}{lg} \qquad \text{Froude number}$$

$$\frac{\text{viscous}}{\text{inertia}} = \frac{\tau}{\rho V^2} \qquad \text{shear/dynamic head}$$

where ρ is the fluid density

V is the representative velocity

ℓ is the representative dimension

μ is the viscosity

p is the pressure

τ is the shear stress

B is the bulk modulus of elasticity

c is the velocity of sound.

In the pipe flow experiments, the elastic (or compressibility) effect and the gravity effect are negligible. The Mach and Froude numbers, therefore, are of little concern. Reynolds' similarity concept mentioned above states that one dimensionless ratio is a function of the others. The number of dimensionless ratios is the sum of the number of related variables and dimensional constants less the number of primary dimensions like length, time, mass, and temperature. For the usual flow conditions, it can be shown that the coefficients $p/\rho V^2$ and $\tau/\rho V^2$ are functions of the Reynolds number alone. The dimensionless drag and lift coefficients of hydrodynamic bodies are a function of Reynolds number alone for wide ranges of application.

TURBULENCE FLUCTUATIONS

Reynolds noted that, as the rate of flow is increased, the flow becomes unstable at a certain Reynolds number. Depending on the quietness of the initial flow, turbulence appears at a higher Reynolds number when instabilities are not damped out, but tends to grow to the state where irregular flow components are present in all directions. The Reynolds number where turbulence first occurs is about 2300, based on the equation:

$$\frac{\rho \bar{u} D}{\mu} = \frac{\bar{u} D}{\nu} \tag{10}$$

where $\bar{u}$ is the mean flow rate

D is the pipe ID

μ is the dynamic viscosity

ν is the kinematic viscosity, μ/ρ

ρ is the fluid density.

Reynolds introduced a method of averaging that is still in use. Turbulent components oscillate in time about the mean value that is steady in time. The mean value is defined by the equation:

$$\bar{u} = \frac{1}{T}\int_{t}^{t+T} u(t)dt \tag{11}$$

where T is a time interval large enough for the mean value to be constant in time t

$u(t)$ is the velocity component at a point in the fluid

$\bar{u}$ is the mean velocity at that point.

The mean values of the turbulent fluctuating velocity and pressure components are zero, since turbulent components are the difference of a velocity from the mean:

$$u = \bar{u} + u' \tag{12}$$

where u is the velocity at a point

$\bar{u}$ is the mean velocity at that point

u' is the fluctuating component at that point.

The mean square values of fluctuating components are not zero, in general. The quadratic mean values are obtained by the equation:

$$\overline{u'^2} = \frac{1}{T}\int_{t}^{t+T} u'^2 dt \tag{13}$$

where $\overline{u'^2}$ is the mean square value of velocity at a point.

The turbulent components are assumed to be continuous throughout the flow, with the fluctuations being small compared to the flow dimensions. Thus, the fluctuating components are assumed to be continuous functions of the distance and time, and the basic equations of mechanics apply during turbulence. The equations are written in terms of the values during turbulence such as $u = \overline{u} + u'$. The mean over time of the equations is taken by the Reynolds' method of averaging. Terms of the first power of the fluctuating components are zero. Additional quadratic terms such as $\overline{u_i u_j}$ appear. Many studies have been made of isotropic turbulence. The mathematics is simple, and many turbulent processes, such as the flow at the center of the pipe, tend to be isotropic. In isotropic turbulence, there is no correlation between components in different directions at a point, and the components are equal:

$$\overline{uv} = \overline{uw} = \overline{vw} = 0 \qquad \overline{u^2} = \overline{v^2} = \overline{w^2} \tag{14}$$

where u, v, and w are the fluctuating velocity components in three orthogonal directions.

For a fluid to have turbulent shearing stresses, there must be correlations between the different components, and such quadratic terms as $\overline{uv}$, $\overline{uw}$, and $\overline{vw}$ are not zero. This occurs in non-isotropic boundary layer flow where the influence of viscosity is of importance. For pipe flow, the correlation between the radial fluctuating component and the axial fluctuating component is:

$$\overline{u_r u_x} = 0 \qquad \text{at pipe center and at wall.}$$

$$\frac{\overline{u_r u_x}}{\sqrt{\overline{u_r^2}}\sqrt{\overline{u_x^2}}} \cong 0.45 \text{ at maximum.} \tag{15}$$

STRESSES IN TURBULENCE

The Navier Stokes equations of motion for a point show stress components due to turbulence in addition to those due to laminar flow. These stresses are called the Reynolds stresses, or the virtual stresses of turbulence. They are the quadratic time mean of the fluctuating components multiplied by the fluid density, and have both normal and tangential components in a boundary layer, u_i^2 and $u_i u_j$ with $i \neq j$. They add the tensor $u_i u_j$ to the stress-strain relation, equation 3, to form the turbulent stress-strain relation. The total stresses for an incompressible turbulent fluid are given in cylindrical coordinates by the equations:

$$
\begin{aligned}
rr \quad \sigma_{rr} &= -P + 2\mu \frac{\partial \bar{U}_r}{\partial r} - \overline{\rho u_r^2} \\
\varphi\varphi \quad \sigma_{\varphi\varphi} &= -P + 2\mu \left(\frac{\partial \bar{U}_\varphi}{r\partial\varphi} + \frac{U_r}{r} \right) - \overline{\rho u_\varphi^2} \\
xx \quad \sigma_{xx} &= -P + 2\mu \frac{\partial U_x}{\partial x} - \overline{\rho u_x^2} \\
r\varphi \quad \sigma_{r\varphi} &= \mu \left(\frac{\partial \bar{U}_\varphi}{\partial r} + \frac{\partial \bar{U}_r}{r\partial\varphi} - \frac{\bar{U}_\varphi}{r} \right) - \overline{\rho u_r u_\varphi} \\
xr \quad \sigma_{xr} &= \mu \left(\frac{\partial \bar{U}_r}{\partial x} + \frac{\partial \bar{U}_x}{\partial r} \right) - \overline{\rho u_r u_x} \\
\varphi x \quad \sigma_{\varphi x} &= \mu \left(\frac{\partial \bar{U}_x}{r\partial\varphi} + \frac{\partial \bar{U}_\varphi}{\partial x} \right) - \overline{\rho u_\varphi u_x}
\end{aligned}
\tag{16}
$$

where $\overline{U}_r$, $\overline{U}_\varphi$, and $\overline{U}_x$ are the mean flow velocities in the radial, tangential, and longitudinal directions

u_r, u_φ, and u_x are the fluctuating turbulent velocities in the radial, tangential, and longitudinal directions

P is the hydrostatic pressure

μ is the dynamic viscosity

ρ is the fluid density.

In order to solve the Navier Stokes equations and the stress-strain relationships for turbulent flows, there must be obtained relations between the mean and the fluctuating components. J. Laufer,[2] P. S. Klebanoff,[3] G. B. Schubauer,[4] and others at the National Bureau of Standards; British fluid mechanicists such as A. A. Townsend;[5] and other scientists, particularly from Holland such as J. O. Hinze,[6] have for many years been conducting both theoretical and experimental studies of boundary layers, especially in air. They have reported relations between the fluctuating and the mean components in terms of nondimensional ratios. These ratios are mainly dependent on the geometry. The energy balance in the boundary layers has also been reported upon very completely.

STRUCTURE OF TURBULENT LAYERS

Turbulence of fluids flowing over solids always leads to dynamic similarity conditions. The law of the wall states that turbulent flow near walls depends on the wall stress and the kinematic viscosity, ν. A boundary layer is composed of a thin region called the laminar sublayer, a constant stress layer, and an outer layer. The laminar sublayer contains turbulent components, but in lesser magnitudes, and its nature is mainly determined by its viscosity and the wall stress. In the constant stress layer, the motion is almost entirely determined by the shear stress and the viscosity. Most turbulence is produced in

or near the region of constant stress. There is energy equilibrium. The turbulent energy dissipation into eddies and eventually into heat is about equal to the local production of turbulence in this region. When the first law of thermodynamics, or the energy equation, is written in terms of the turbulent quantities (the mean plus the fluctuations), the energy equation can be separated into mean flow and turbulent equations. These equations, like the first law, are energy balances equating the sum of all the components at a point to zero. Figure B-1 shows the energy balance of mean motion in a boundary layer along a smooth wall with zero pressure gradient. There is interaction between the inner and outer parts of the boundary layer. In the outer region, mean flow kinetic energy is

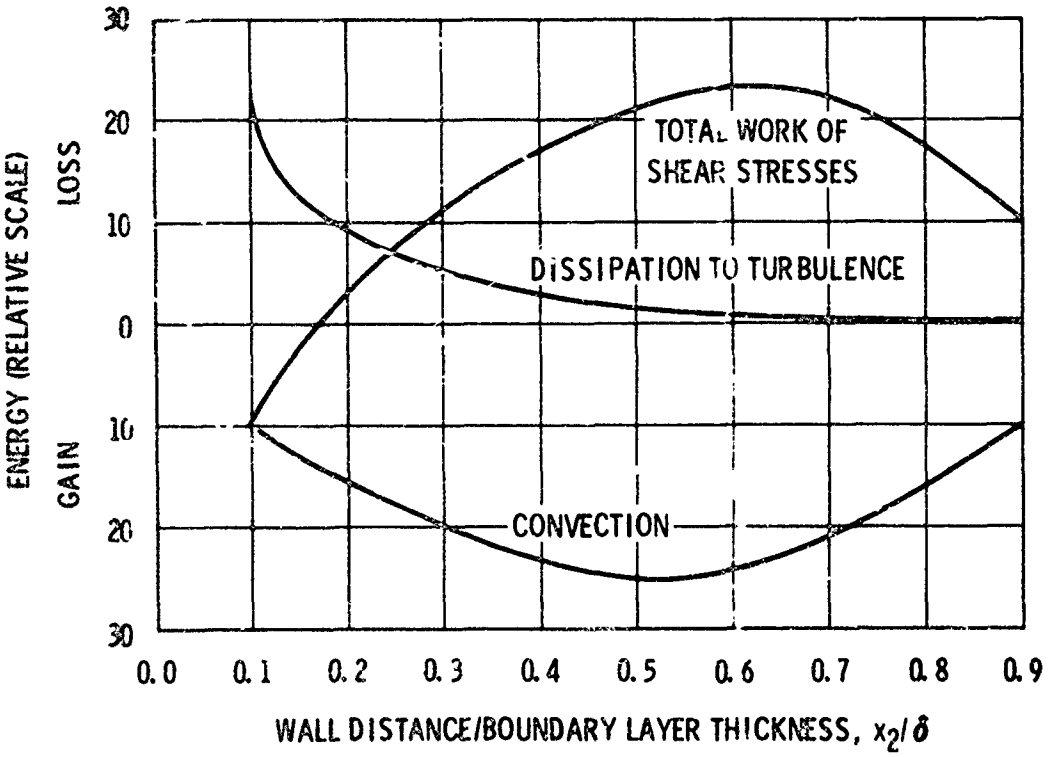

Figure B-1. Energy balance of mean motion in a boundary layer along a smooth wall with zero pressure gradient (adapted from ref. 5).

retarded by the work of the turbulent shear stresses. The gain to the mean motion by convection is about equal to that lost by the turbulent shear stress work. The production of turbulence is small in the outer region, but it increases strongly toward the wall. In the inner region, the production of turbulence exceeds that due to convection, with the difference being made up by the work of turbulent shear stresses. There is an influx of energy toward the wall where it is converted mainly into turbulence energy, originating from the mean motion, but is in part diffused back by turbulence into the outer region. Figure B-2 shows the turbulent energy balance in a pipe at the wall region. The energies of dissipation into heat, viscous transfer of kinetic energy, production of turbulent energy, and the diffusion of kinetic and pressure energies are shown.

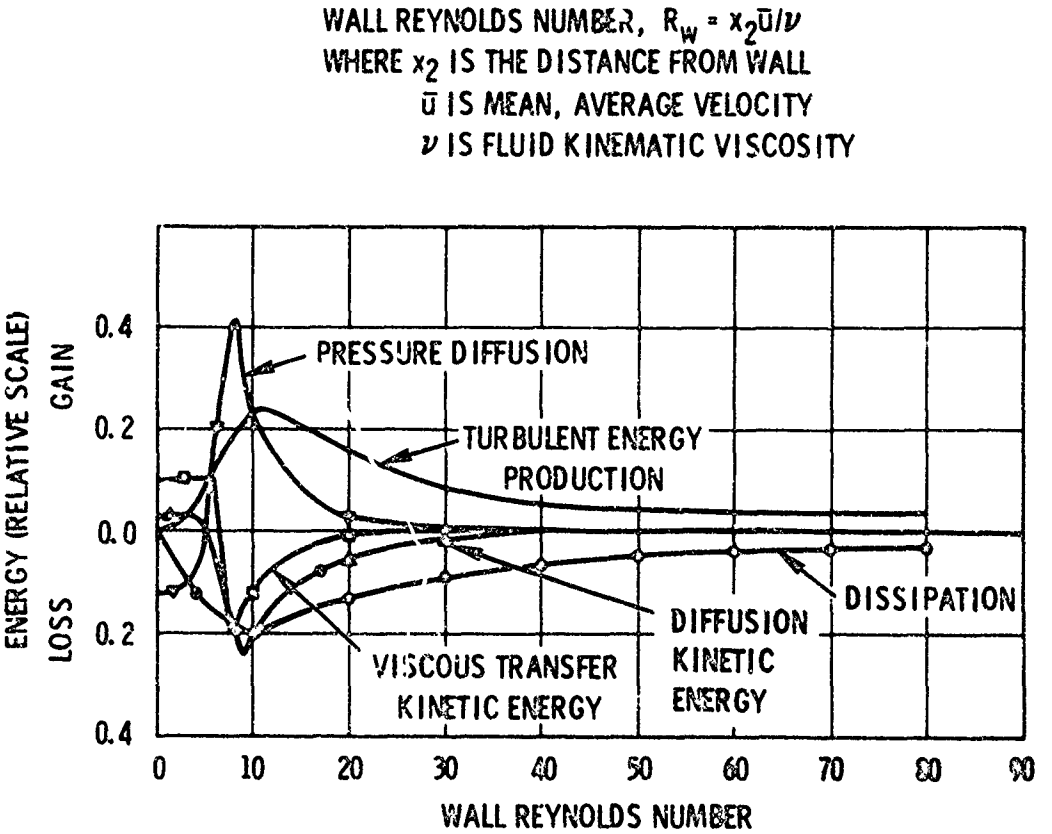

Figure B-2. Energy balance in wall region of pipe flow.

Close to the wall, all of the terms are of importance; dissipation and production are nearly equal, but opposite in algebraic sign, as are terms representing diffusion of kinetic energy and pressure energy. Further from the wall, the main terms in the energy balance are the production and the dissipation with some turbulent diffusion. In the outer region of energy, balance is between the turbulent diffusion energy and the dissipation. The peak values of the terms occur at the wall end of the constant stress region at distances corresponding to wall Reynolds numbers less than 10 based on the wall distance and the friction velocity, $x_2 u/\nu$. The friction velocity is defined by the equation

$$\tau_w = \rho u_*^2 = \frac{\Delta P r}{L 2} \tag{17}$$

where τ_w is the wall stress

ρ is the fluid density

u_* is the friction velocity

ΔP is the pressure drop in the length L

r is the pipe radius.

Wall Reynolds numbers of about 8 have been called the end of the laminar sublayer. The constant stress layer of energy equilibrium extends from the end of the laminar sublayer to Reynolds numbers of about 100. Figure B-3 summarizes figuratively what happens to the energy flow in a boundary layer, indicating the extraction of the energy of mean flow and its transfer in the direction of the wall. The greatest production and dissipation are shown to occur near the wall. The turbulent diffusion of energy toward the outer region is also shown.

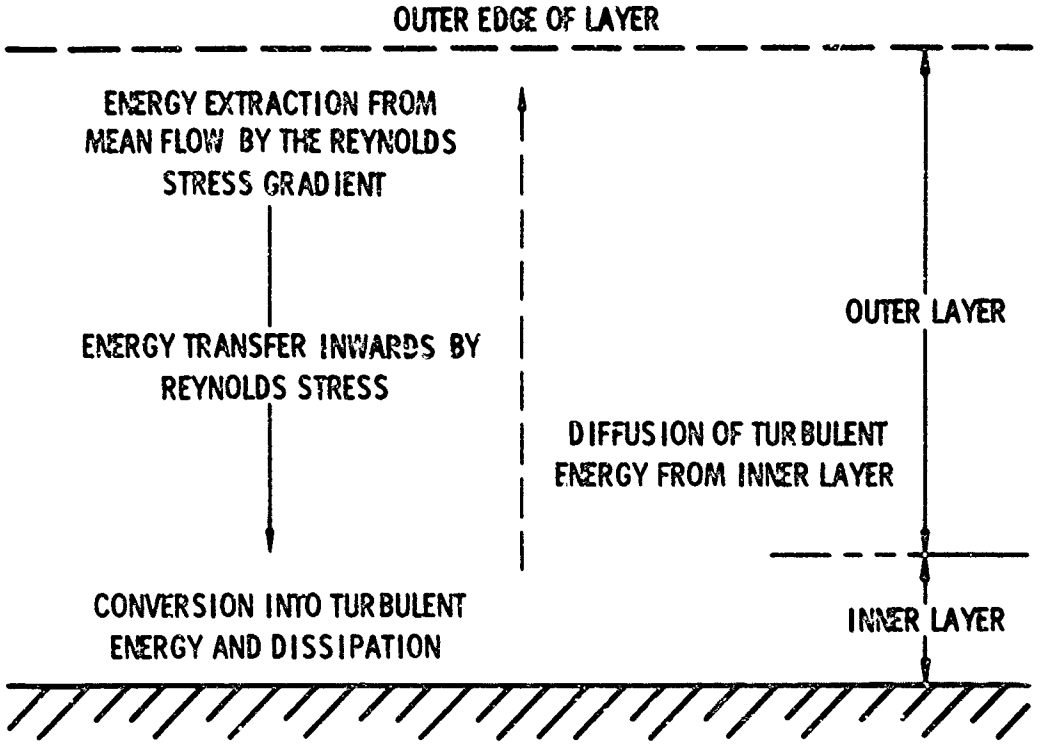

Figure B-3. Energy flow in a boundary layer.

TURBULENCE COMPONENTS

The experimental studies of Laufer and others indicate that the velocity ratios are mainly a function of the geometry and are nearly constant in the constant stress region. Figure B-4 shows the ratios of the fluctuating components to the maximum mean axial velocity plotted against the wall distance radius ratio, x_2/r. Figure B-5 shows the ratios of the fluctuating components to the friction velocity plotted against the wall Reynolds number, $x_2 u_* / \nu$. These velocity ratios are nearly constant in the constant stress region.

WALL DISTANCE/RADIUS x_2/r

WHERE U IS THE MAXIMUM MEAN VELOCITY

x_2 IS THE DISTANCE FROM THE PIPE WALL

r IS THE PIPE RADIUS

u_r IS THE FLUCTUATING RADIAL TURBULENT VELOCITY

u_ϕ IS THE FLUCTUATING TANGENTIAL TURBULENT VELOCITY

u_x IS THE FLUCTUATING LONGITUDINAL TURBULENT VELOCITY

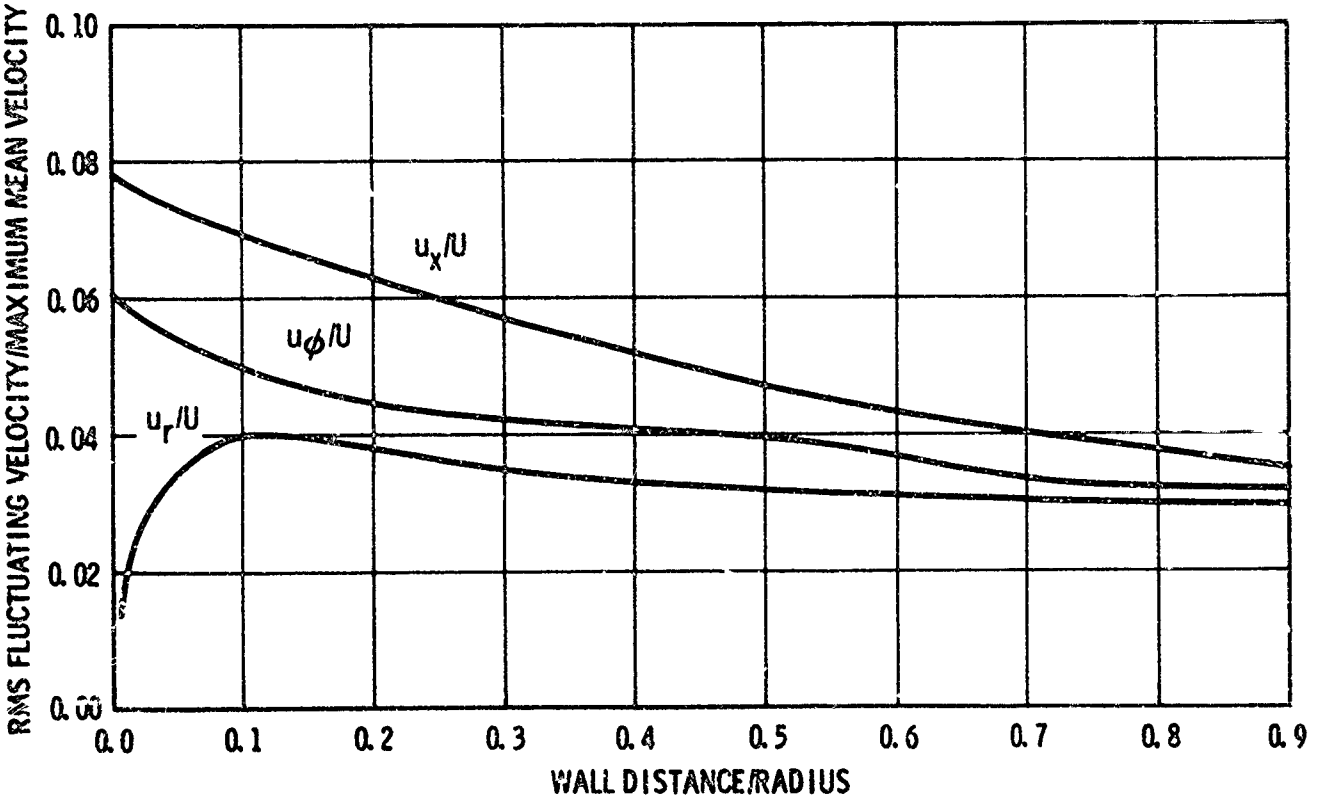

Figure B-4. Relative turbulent intensities in pipe flow (adapted from ref. 2).

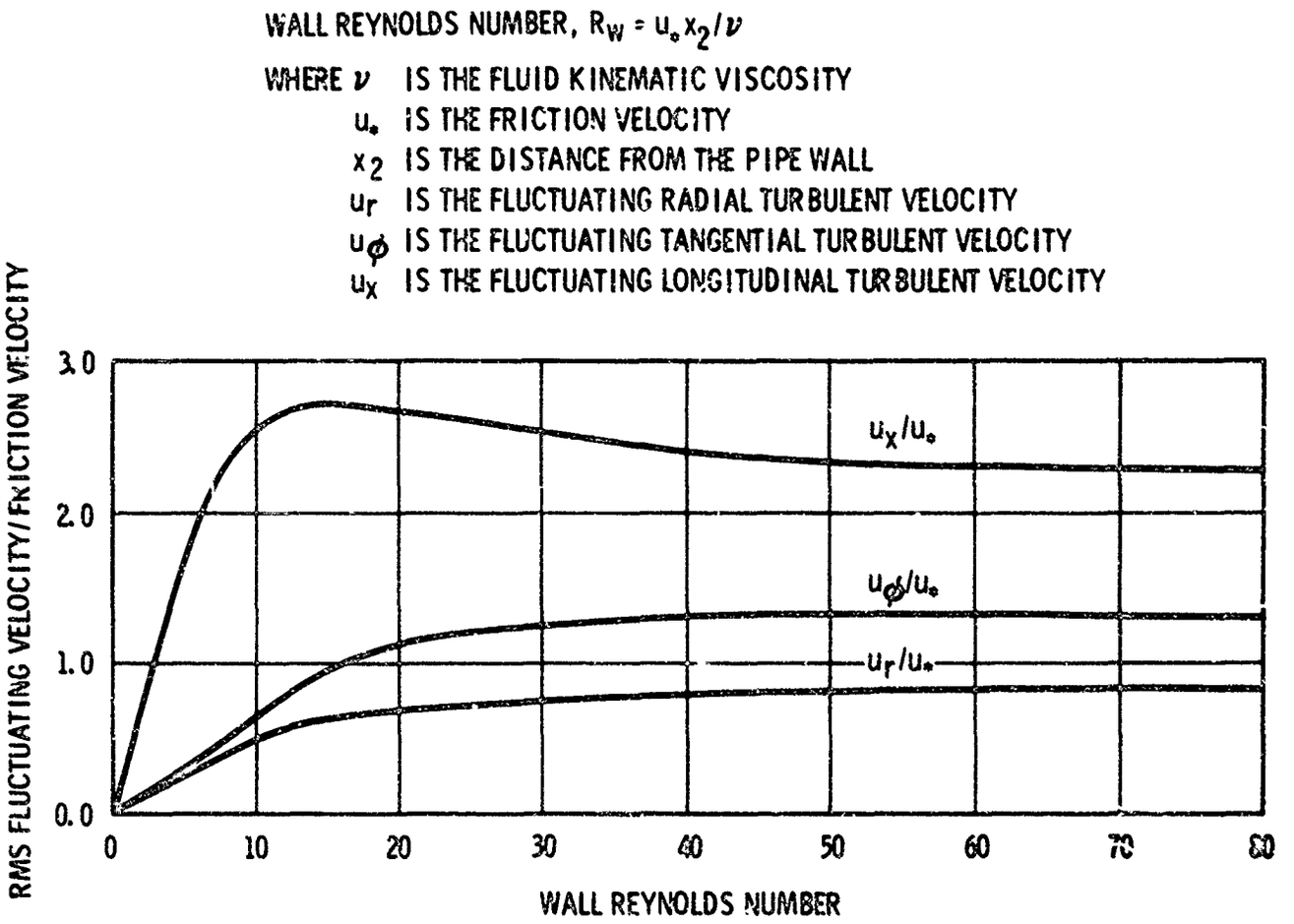

Figure B-5. Turbulent intensities near the wall in pipe flow (adapted from ref. 2).

The distribution of the turbulence shear stress is of interest. The shear stress/friction velocity ratio, $\overline{-u_x u_r}/u_*^2$ is plotted for pipe flow near the pipe wall (fig. B-6). The correlation coefficient for shear components can be approximated from the velocity ratios of figure B-4 and from the shear stress/friction velocity ratios of figure B-5. The velocities are the rms fluctuations for the components:

$$\frac{\overline{u_r u_x}}{u_*^2} = \frac{u_r}{u_*} \cdot \frac{u_x}{u_*} \qquad \frac{\overline{u_r u_x}}{u_r u_x} = \frac{u_r}{u_*} \frac{u_x}{u_*} R_{rx}$$

or

$$R_{Rx} = \frac{\overline{u_r u_x}}{u_*^2} \cdot \frac{u_* u_*}{u_r u_x} = \frac{.9}{.8 \times 2.5} = .45 \qquad (18)$$

WALL REYNOLDS NUMBER, $R_W = u_* x_2 / \nu$
WALL STRESS/FRICTION VELOCITY, $-\overline{u_x u_r}/u_*^2$
WHERE ν IS THE FLUID KINEMATIC VISCOSITY
u_* IS THE FRICTION VELOCITY
x_2 IS THE DISTANCE FROM THE PIPE WALL
u_x IS THE FLUCTUATING LONGITUDINAL TURBULENT VELOCITY
u_r IS THE FLUCTUATING RADIAL TURBULENT VELOCITY

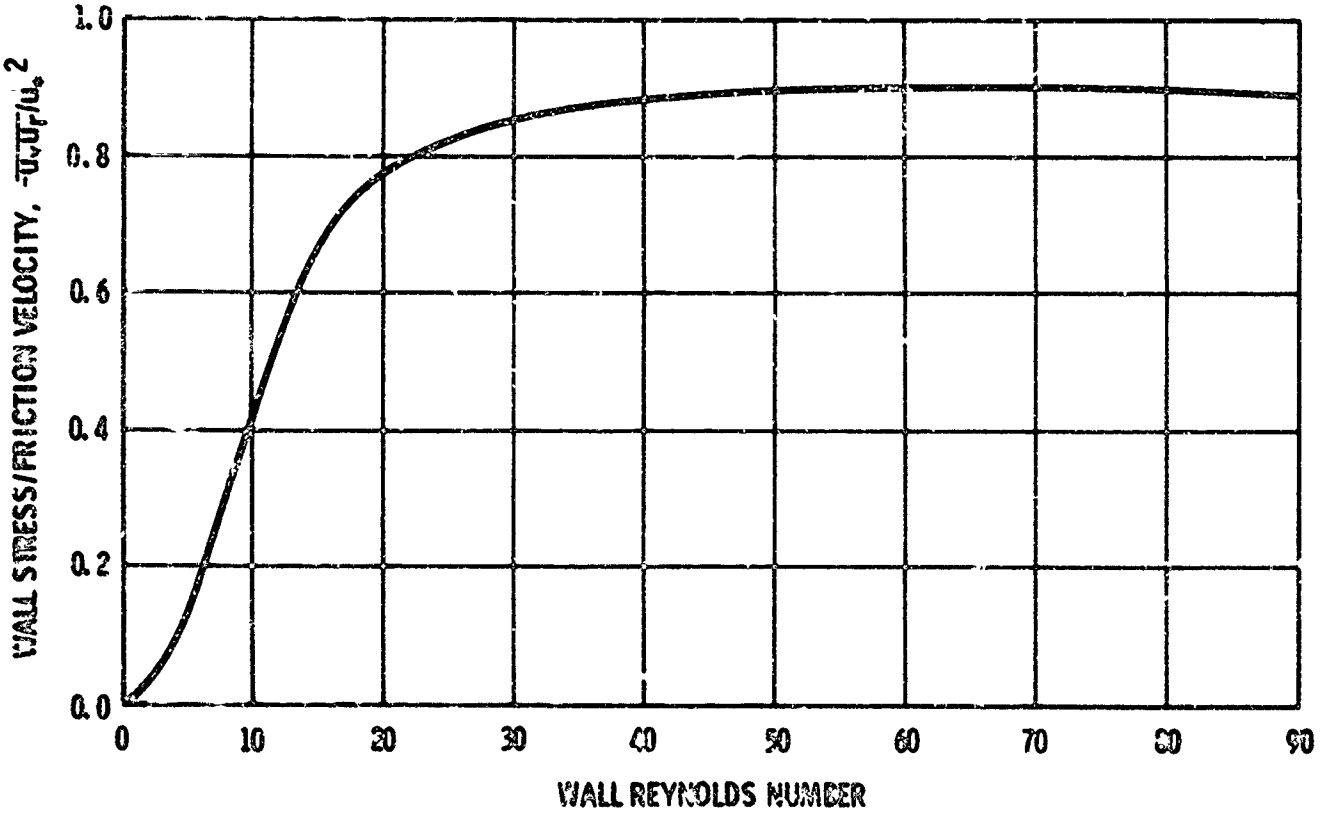

Figure B-6. Distribution of turbulence shear stress near the wall in pipe flow (adapted from ref. 2).

The correlation coefficient for the shear is equal to approximately 0.45 over most of the pipe. The ratio of twice the sum of the turbulent kinetic energies, $u_i u_i$, or q_i^2, and the shear stress, $\overline{-u_r u_x}$, is nearly constant over most of the pipe. Figure B-7 is a plot of this ratio, $\overline{-u_x u_r}/q_i^2$, against the wall distance/radius ratio, x_2/r.

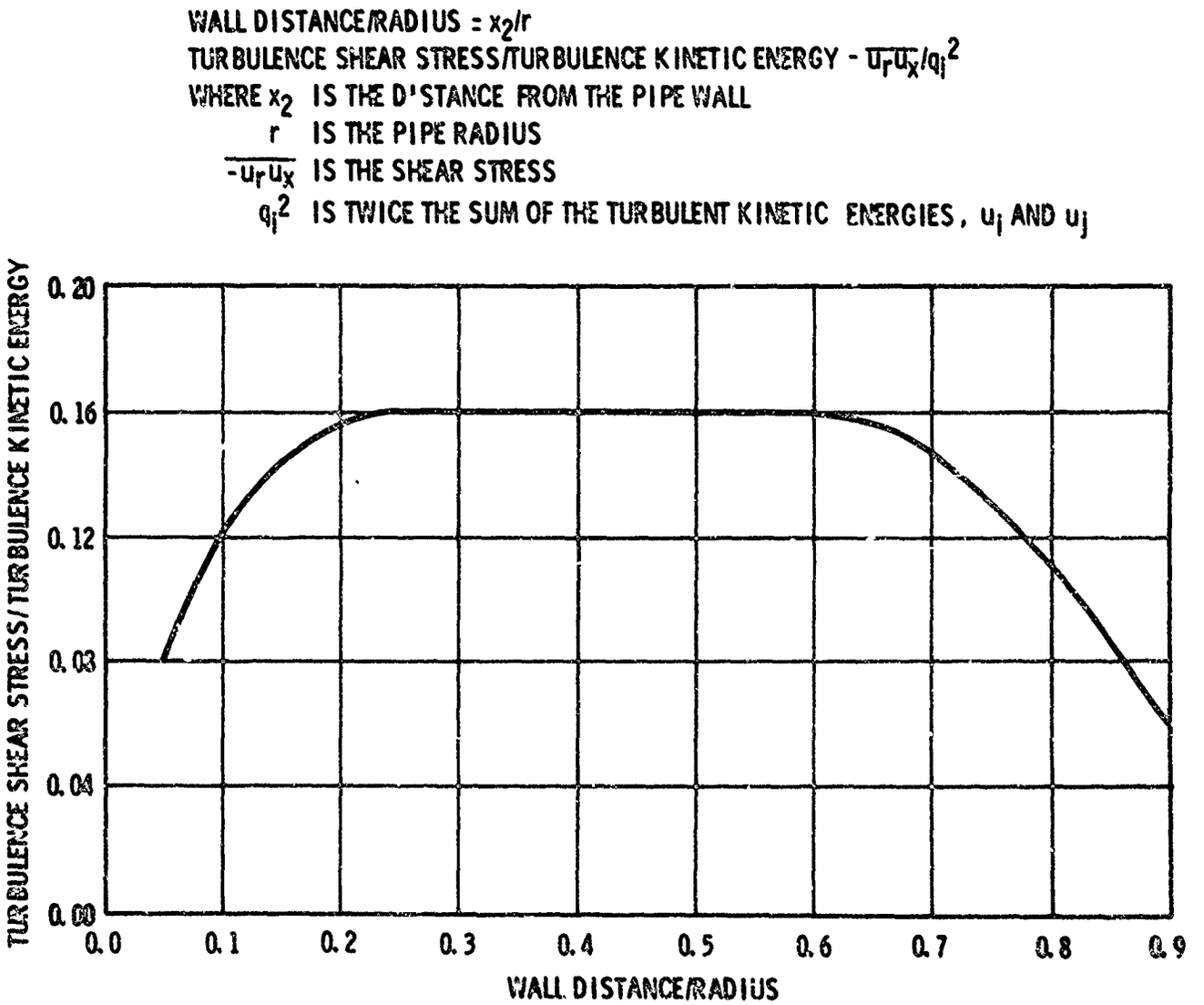

Figure B-7. Ratios between turbulence shear stress and turbulence kinetic energy in pipe flow (adapted from ref. 2).

Figure B-8 shows the turbulent kinetic energy and the turbulent shear stress, $\overline{-u_r u_x}$, plotted against the wall distance/radius ratio.

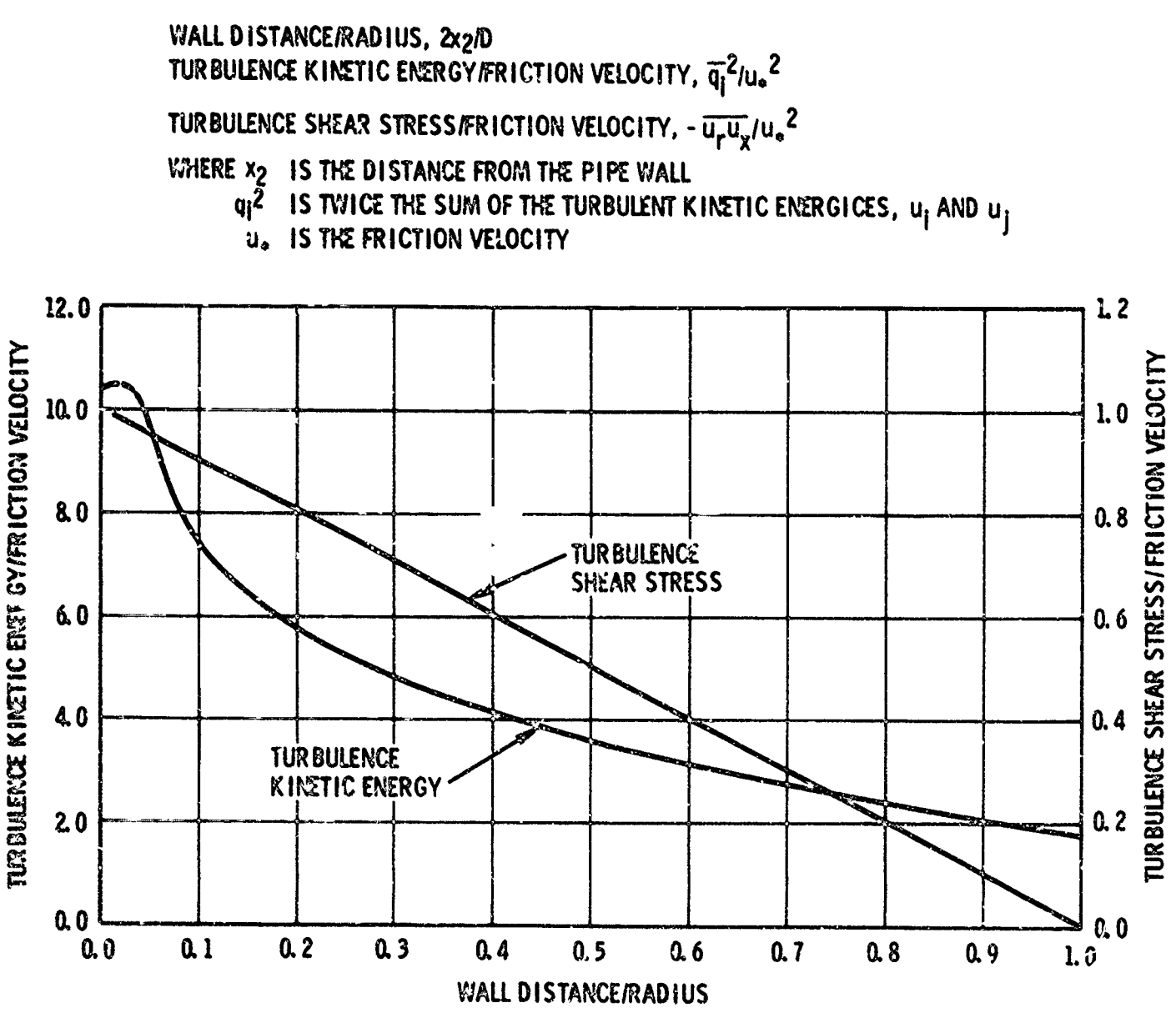

Figure B-8. Distribution of turbulence kinetic energy and turbulence shear stress in pipe flow (adapted from ref. 2).

PRESSURE/DYNAMIC HEAD RATIO

The experimental test hydrophones measured the fluctuating component of the normal stress, σ_{rr}, at the cylindrical pipe wall: $\sigma_{rr} = -\rho\overline{u_r^2}$. Laufer was able to measure the distribution of the $\overline{u_r q^2}$ accounting for the viscous transfer of kinetic energy toward the wall in the energy balance. The diffusion of the pressure energy toward the wall is the closing balance in the pipe flow energy balance curves of figure B-2. The normal fluctuating pressure component at the wall can be expected to approximate that in the constant pressure layer.

Willmarth measured the wall pressure fluctuations at the wall in a 4-inch ID wind tunnel to speeds of Mach 0.8.[7] His measurements are given in terms of the ratio between the fluctuating rms pressure and the dynamic head, $\frac{1}{2}\rho U^2$, with U being the free-stream velocity outside the boundary layer. The ratio, $p/\frac{1}{2}\rho U^2$, has a nearly constant value of 0.0035 over the Mach number range. (Theoretical justification of the constant ratio is not attempted by Willmarth: the normal fluctuating pressure must be primarily related to the wall stress.) There is a viscous transfer of kinetic energy toward the wall from the constant stress layer, and the pressure energy is also transferred toward the wall. The fluctuating normal pressure in the radial direction should be nearly the same at the wall and at the constant stress layer. Ratios of the same general magnitude as that of Willmarth are obtained from Laufer's velocity ratio measurements.

If the ratio of $\rho u_r^2 / \frac{1}{2}\rho U_m^2$ is obtained from the ratios between the rms radial velocity fluctuation and the maximum mean flow velocity, U_m, taken from figure B-4, a rms wall pressure to dynamic pressure ratio results:

$$p/\bar{q} = \frac{2u_r^2}{U_m^2} = 2 \times 0.04^2 = 0.0032 \qquad (19)$$

For a mean flow velocity distribution across the pipe of 1/7th power, the ratio of the average mean flow rate to the maximum mean flow rate is 0.817. The wall pressure/dynamic head ratio based on the average flow velocity is $p/q = 0.0032/0.817^2 = 0.00478$, using figure B-4.

The wall stress/dynamic head dimensionless ratio can also be used to evaluate the fluctuating pressure to dynamic head ratio, p/q. The wall stress/inertia head ratio, τ/q, is nearly a constant over all the experimental measurements, but is a function of the Reynolds number. Figure B-5 shows the radial velocity/shear velocity ratios that can be used to obtain the p/q ratios:

$$p/q = \frac{\tau_w}{q} \times \frac{u_r^2}{u_*^2} \tag{20}$$

since $\tau_w = \rho u_*^2$, where u_r/u_* is obtained from figure B-5 and is assumed to be ~ 0.9. It is assumed above that the normal fluctuating pressure at the wall is determined by the kinetic energy transported from the constant stress layer without much change, $p = \rho u_r^2$. For an approximate ratio of wall stress/dynamic head of 0.0075 for a Reynolds number of 15,000, the p/q ratio would be $0.0075 \times 0.9^2 = 0.00608$.

Innumerable experimental measurements of wall friction in pipe flow have been made over many years; the wall stress per unit area is given in terms of the dynamic head and a friction coefficient: $\tau_w = f\rho\bar{u}^2/2$ where $\bar{u}$ is the average mean velocity, and f is the friction coefficient, or the ratio τ_w/q.

Many experimenters like Nikuradse[8] have obtained relationships with the friction coefficient and Reynolds number. H. Blasius[9] suggested a simple relationship that is accurate for Reynolds numbers from 3000 to 100,000: $f = 0.079R^{-1/4}$ where f is the friction coefficient or τ_w/q ratio, and R is the Reynolds number based on the average velocity and the pipe diameter, $\bar{u}D/\nu$. Thus, the p/q ratio can be estimated at the wall from the friction coefficient and the velocity ratio, u_r^2/u_*^2, by the equation:

$$p/q = f \cdot \frac{u_r^2}{u_*^2} \tag{21}$$

For the water pipe flow experiment, broadband fluctuating pressures were recorded on all the test runs. This noise, recorded on magnetic tapes, was analyzed with Sanborn equipment to obtain broadband rms magnitudes. Broadband rms magnitudes were also obtained by numerical integration of the spectrum levels. Since random pressures combine as the sum of their squares, the numerical integration was performed by dividing the frequencies into narrow bands, in which the spectrum level was relatively constant, and adding up the sum of the squares by:

$$P^2 = p_{s_1}{}^2 \Delta f_1 + p_{s_2}{}^2 \Delta f_2 + p_{s_3}{}^2$$

$$= p_{s_1}{}^2 \Delta f_1 \left[1 + \left(\frac{p_{s_2}}{p_{s_1}} \right)^2 \frac{\Delta f_2}{\Delta f_1} + \left(\frac{p_{s_3}}{p_{s_1}} \right)^2 \frac{\Delta f_3}{\Delta f_1} \right] \tag{22}$$

where p_{sn} is the rms spectrum level or per cycle bandwidth level

f_n is the bandwidth over which the spectrum is nearly constant

P is the rms broadband pressure.

The ratios of the broadband rms magnitudes to the dynamic head are presented, for magnitudes obtained by the various methods, in figures 16 and 17.

TURBULENCE DISSIPATION

Much of the knowledge of turbulence is due to the experimentalists. The equations in terms of the mean and fluctuating components usually cannot be solved without relationships between them. Various experimental ratios of fluctuating to the mean components as a function of the wall distance have been discussed. The energy balances must

be made with measured terms. The most complete and reliable measurements with turbulent ...ities are the pipe measurements of Laufer. His mea... ...its were made in air at speeds of 3 and 30 meters per second maximum mean velocity, corresponding to Reynolds numbers of 50,000 and 500,000 based on the maximum average velocities and the pipe diameter (9.72 inches ID). By a hot wire anemometer technique, he was able to measure triple velocity correlations such as $\overline{u_r^3}$, $\overline{u_x^2 u_r}$, and $\overline{u_\varphi^2 u_r}$ to obtain terms for the energy balance equation. He measured the

velocity derivatives $\left(\overline{\frac{\partial u_x}{\partial x}}\right)^2$, $\left(\overline{\frac{\partial u_r}{\partial x}}\right)^2$, and $\left(\overline{\frac{\partial u_\varphi}{\partial x}}\right)^2$ and,

by assuming local isotropy, he was able to evaluate turbulence dissipation. Figure B-9 shows the turbulence dissipation in pipe flow based on Laufer's measurements, expressed in nondimensional numbers as $\epsilon' D / 2u_*^3$ where ϵ' is the dissipation, D is the pipe diameter, and u_* is the friction velocity. This quantity has a value of approximately 22 at 1/10 radius from the pipe wall; for greater distances, it varies hyperbolically with distance from the wall. The average value appears to be about 11 if the dissipation coefficient remains the same for points nearer the wall than 1/10 radius (the dissipation was not measured in the constant stress layer which is nearer the wall). Laufer's values are a careful evaluation of the dissipation for isotropy of the dissipation tensor, $\nu \overline{\partial u_j \partial u_j / \partial x_i \partial x_i}$. The values give local dissipation for points in the pipe outside the region near the wall.

Laufer's values of the dissipation function can be compared with the shear measurements of the water pipe flow experiment. If one assumes that the viscous dissipation is small compared to turbulence dissipation (as can be expected at higher Reynolds numbers), the shear power at the wall can be assumed to be equal to the turbulence dissipation in the corresponding volume:

$$\epsilon_A' \pi r^2 L = \tau_w \frac{dL}{dt} 2\pi r L \qquad \epsilon_A' = \frac{2}{\rho r} \tau_w \frac{dL}{dt} = \frac{L^2}{T^3} \tag{23}$$

REYNOLDS NUMBER, R = UD/ν = 50,000
WALL DISTANCE/RADUIS = $2x_2/D$
TURBULENCE DISSIPATION = $\epsilon' D/2u_*^3$
WHERE U IS THE MAXIMUM MEAN VELOCITY
D IS THE PIPE INSIDE DIAMETER
ν IS THE FLUID KINETIC VISCOSITY
x_2 IS THE DISTANCE FROM THE PIPE WALL
ϵ' IS THE DISSIPATION IN L^2/T^3
u_* IS THE FRICTION VELOCITY

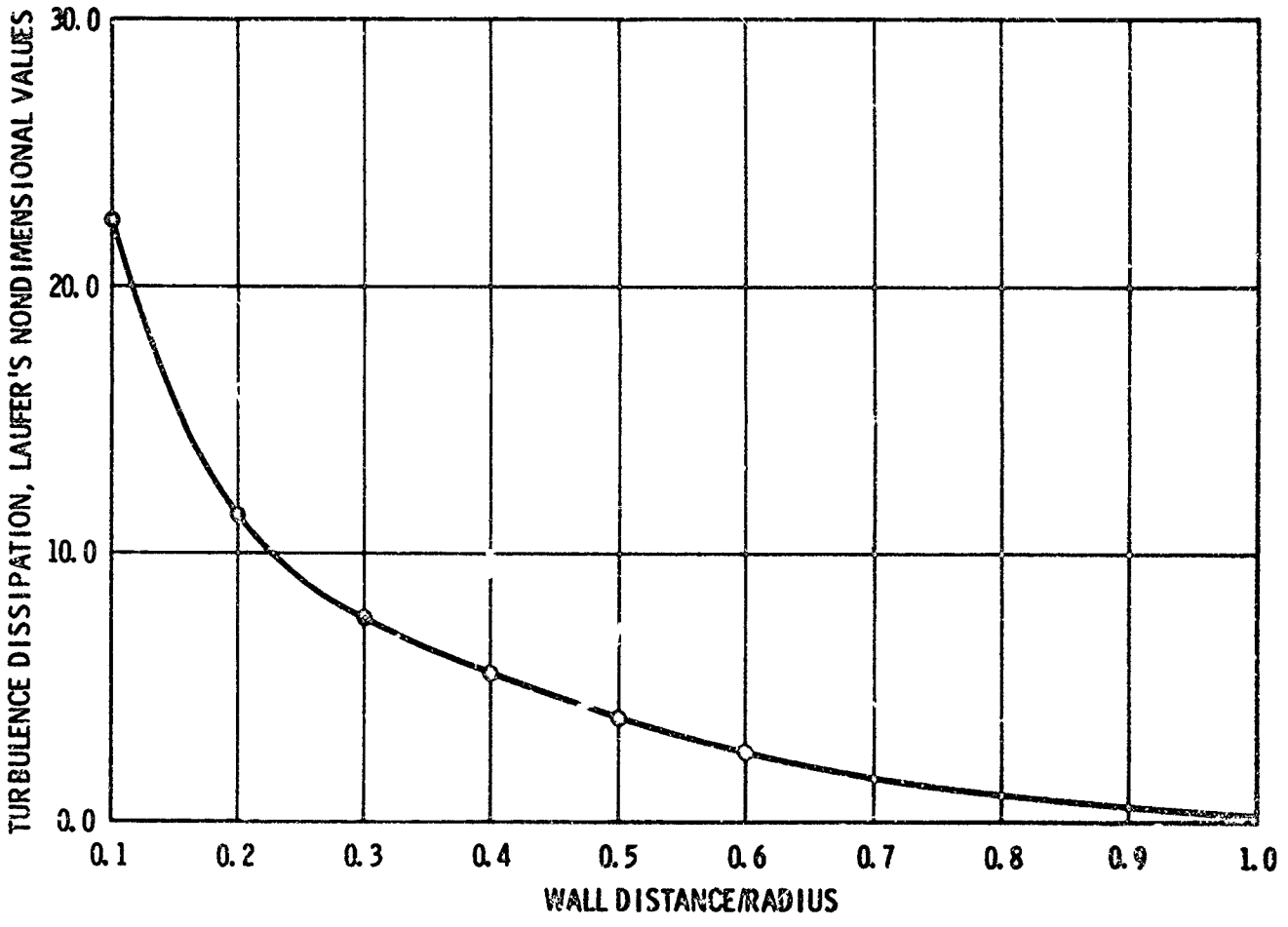

Figure B-9. Turbulence dissipation in pipe flow (adapted from reference 2).

where ϵ_A' is the average power dissipation per unit mass

τ_ω is the wall shear stress

r is the pipe radius

L is the pipe length from the velocity expression dL/dt

ρ is the mass density of the fluid ($\rho = m/V$)

L^2/T^3 is the dimension of turbulence dissipation which is a kinematic quantity of energy per unit time per unit mass.

The equation above states that the average dissipation is directly proportional to the wall shear power as expected. In figure B-10, ϵ_A' is plotted against wall shear power for water flow at 7.5 fps through a 0.494-inch ID pipe, with a measured wall shear stress of 0.396 pounds per square foot and a mass density equal to 62.422 lb/ft^3 divided by 32.174 ft/sec^2. The turbulence dissipation for these conditions is 148/63 ft^2/sec^3. The nondimensional dissipation coefficient (defined by Laufer as $\epsilon' D/2u_*^3$) which corresponds to this friction velocity and dissipation value is 32.7. This is of the order of magnitude of Laufer's values.

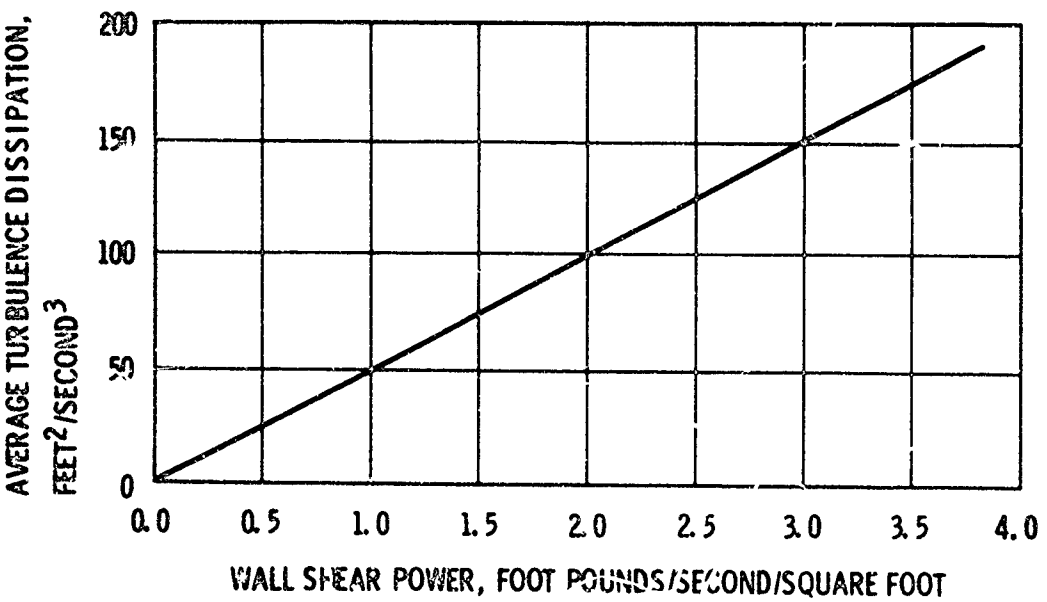

Figure B-10. Approximate turbulence dissipation in a 0.494-inch ID pipe.

SOUND POWER

A portion of the fluctuating turbulence power can be called sound power. Sound power per unit area, or the intensity of a sound wave, is defined as the average rate of flow of sound energy. For the turbulent components, the intensity is the correlation between the fluctuating pressure and the velocity component in the same direction. The sound intensity in the radial direction is the term $\overline{p_r u_r}$ or $\overline{\rho u_r^3}$. Laufer measured the triple velocity correlation, $\overline{u_r^3}/u_*^3$, over the pipe and gives a value of 0.45 over most of the wall distances. An index of sound power can be obtained from the ratio of the radial sound intensity to the average friction power:

$$\frac{\overline{p_r u_r}}{\tau_w \overline{U}} = \frac{\overline{u_r^3}}{\tau_w \overline{U}} = \frac{\overline{u_r^3} u_*^3}{\tau_w \overline{U} u_*^3} = \frac{\overline{u_r^3}}{u_*^3} \frac{u_*}{\overline{U}} = \frac{\overline{u_r^3}}{u_*^3} \sqrt{\frac{F}{2}} = \sim 0.026 \qquad (24)$$

where τ_w is the wall friction stress, $\rho u_*^2 = \tau_w$

f is the wall friction factor

$\overline{U}$ is the average mean velocity

u_r is the radial velocity component rms.

This sound power ratio was measured to be 0.026 as an average for the water pipe flow test runs.

The intensity of the radiated sound due to turbulence was discussed by M. J. Lighthill in his classic papers in the Proceedings of the Royal Society of London.[10,11] By approximating for the covariances in Lighthill's expression for the radiated intensity, Proudeman has obtained an equation for the radiated power per unit volume for isotropic turbulence.[12] Proudeman considers the equation representative at higher Reynolds numbers:

$$P = \frac{38\rho(u'^2)^{5/2}\epsilon'}{c^5} \tag{25}$$

where P is the radiated power per unit volume

ϵ' is the dissipation per unit mass

c is the velocity of sound in the medium

u' is the fluctuating velocity component.

RADIATED POWER

The portion of the wall shear power radiated as sound can be estimated roughly using the average dissipation and Proudeman's equation. The fraction of the power radiated is:

$$\frac{\dfrac{38\rho(u'^2)^{5/2}\pi r^2 L\epsilon_A'}{c^5}}{\tau_w 2\pi r L\dfrac{dL}{dt}} = \frac{\dfrac{38\rho\,(u'^2)^{5/2}\,2\tau_w dL\pi r^2 L}{c^5\,\rho r\,dt}}{\tau_w 2\pi r L\dfrac{dL}{dt}} = \frac{38(u'^2)^{5/2}}{c^5} \tag{26}$$

It can be seen that, according to this formula, the fraction of power radiated into sound is very small, except for high fluctuating velocities. For a fluctuating velocity of 10 centimeters per second (corresponding to a water flow rate of 30 pounds per minute through the test pipe) and with the velocity of sound in water of 1.48×10^5 centimeters per second, the fraction radiated into sound is $28(10/1.48\times10^5)^5 = 0.53\times10^{-20}$.

HARMONIC ANALYSIS

All of the pressure fluctuations of this report were measured at one point of the hydrophone output at the pipe wall. The photographs of both the hydrophone and the micrometer outputs show the random nature of the pressure fluctuations. The waveform is constantly changing its shape with time and never exactly repeats itself within finite time. The infinite number of waveforms is called an ensemble. Functions of this type are described by statisticians in terms of probability distributions for the instantaneous values to arrive at statistical averages. The averages of this analysis are values measured by techniques based on harmonic analysis. Generalized harmonic methods are suitable for analyzing most functions such as periodic, transient or aperiodic, and random functions. It has been mentioned earlier that turbulence is primarily described by a representative velocity, a representative length, space and time correlations, and power spectra. The present analysis principally gives the broadband rms magnitude which is related to the velocities, and the power spectra. Autocorrelations are also analyzed. They play a central role in the general harmonic theory. The power spectra are obtainable without the autocorrelations. Harmonic analysis is based on the assumption by the Wiener theorem that autocorrelations exist for the functions and that a common autocorrelation exists for all the members of the ensemble. This means that all members of an ensemble have the same power spectrum regardless of the waveform. Due to the fluctuating nature of turbulence with zero mean values, and because the relationships are usually between two quantities expressed as a product, the variables of the analysis are mostly in quadratic terms such as the mean squared values, the power spectra, and the correlations (the broadband values were discussed in conjunction with pressure/dynamic head ratios).

CORRELATIONS DEFINED

The correlations between quantities in flow have been shown to be tensors by de Karman and Howarth.[13] Correlations in a steady flow are between fluctuating vector components integrated, as a product over a sufficiently long time period, to the correlation independent of time:

$$R_{ij}(x,r) = \lim_{T\to\infty} \frac{1}{T} \int_0^T u_i(x)u_j(x+r)dt \qquad (27)$$

where $R_{ij}(x,r)$ is the correlation between vector components i and j displaced by a vector distance r

$u_i(x)$ is the instantaneous value at point x of the i component of the fluctuating vector velocity

$u_j(x,r)$ is the instantaneous value of the fluctuating vector j component at the point displaced r from the point x

T is the interval of integration.

Correlations in flow have been defined in various manners. Figure B-11 shows some of the definitions. In 1937, de Karman and Howarth defined longitudinal correlation as the correlation between components at points A and B in the same direction as the line between the points. Lateral correlation is defined as that between two components at right angles to the direction between points A and B. Taylor's experimental measurements were made with hot wires which responded mainly to components in the direction of flow in the wind tunnel.[14,15] Taylor's longitudinal correlation is between velocity components in the direction of the main flow at two points located in a line in the main flow direction. Taylor's lateral correlation is between components in the main flow direction but displaced at right angles to the tunnel. Harrison at David Taylor Model Basin and Von Winkle at the U. S. Navy Underwater Sound Laboratory relate pressure values at the wall in their wind tunnels.[16,17] Pressure correlations are called longitudinal

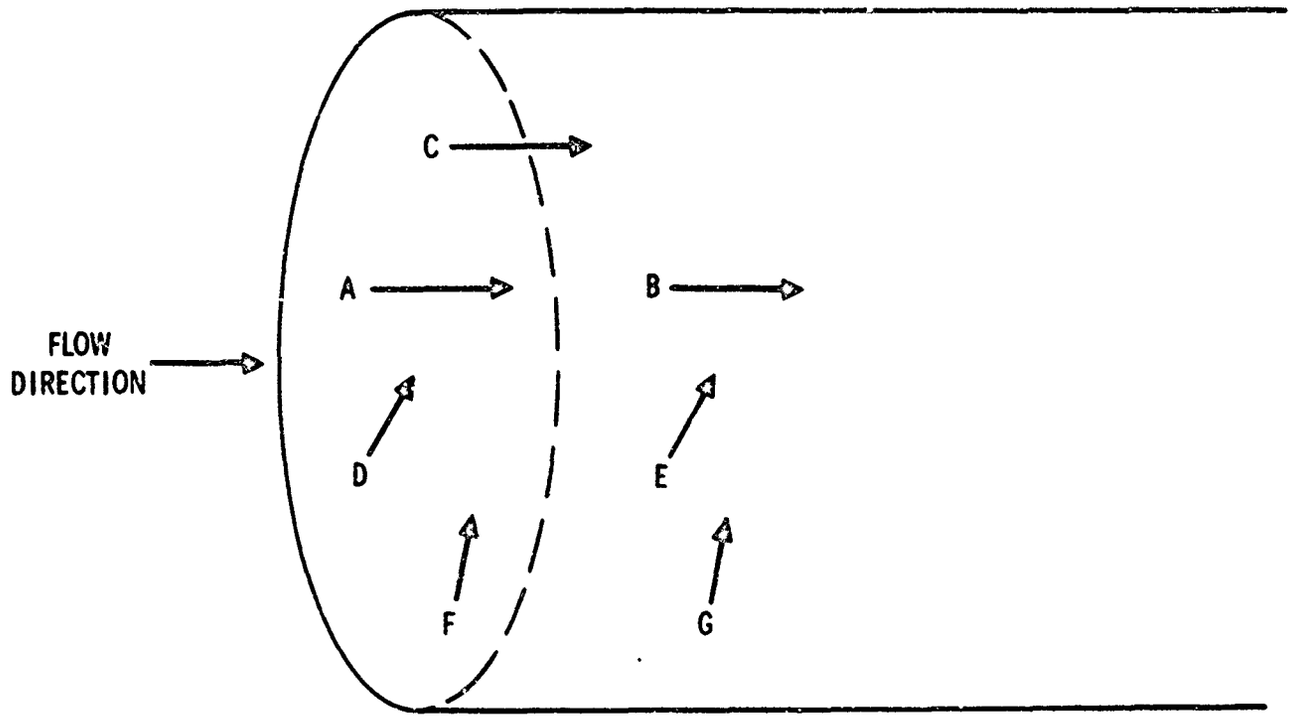

TYPE CORRELATION	EXPERIMENTALISTS' DEFINITIONS			BETWEEN POINTS
	EXPERIMENTER	CORRELATION	PRESSURE COMPONENT	
LONGITUDINAL: COMPONENTS ARE PARALLEL TO DIRECTION OF DISPLACEMENTS	de KÁRMÁN & HOWARTH	LONGITUDINAL	LONGITUDINAL	A TO B
	TAYLOR	LONGITUDINAL	LONGITUDINAL	A TO B
LATERAL: SINCE PRESSURE COMPONENTS ARE NORMAL TO THE DIRECTION OF THE DISPLACEMENTS	de KÁRMÁN & HOWARTH	LATERAL	NORMAL TO WALL	D TO E
	TAYLOR	LATERAL	LONGITUDINAL	A TO C
	HARRISON	LONGITUDINAL	NORMAL TO WALL	D TO E
		TRANSVERSE	NORMAL TO WALL	D TO F
	VON WINKLE	LONGITUDINAL	NORMAL TO WALL	D TO F
		LATERAL	NORMAL TO WALL	D TO F
	LAITINEN	AUTOCORRELATION	NORMAL TO WALL	G TO G

Figure B-11. Sketch of space correlations for pipe flow.

for points in the direction of tunnel flow. Harrison calls correlations between wall points at right angles to the tunnel transverse correlations, while Von Winkle calls them lateral correlations. If it is assumed that the wall pressures are normal to the wall, both the longitudinal and the lateral (transverse) pressure correlations are of the lateral type as defined by de Karman and Howarth, since the components are normal to the direction of the displacements. These pressure correlations show principally how the fluctuating wall pressure is related along the wall surface. It can be expected that longitudinal pressure correlations are over larger distances than the lateral pressure correlations, since the main flow is convected in the longitudinal (tunnel) direction.

For zero displacement distance, the nondimensional correlation of shear stress, obtained by dividing the products of the rms magnitudes, has been mentioned as being equal to approximately 0.45 over most of the pipe radii:

$$R_{rx} = \frac{\overline{u_r u_x}}{\sqrt{\overline{u_r^2}}\sqrt{\overline{u_x^2}}} = 0.45 \tag{28}$$

The correlations of this report are autocorrelations. They correlate the pressure components at the same point and in the same radial direction, but differing in the time separation or lag between them:

$$R(\tau) = \lim_{T\to\infty} \frac{1}{2T}\int_{-T}^{T} P(t)p(t+\tau)dt \tag{29}$$

where $R(\tau)$ is the autocorrelation between the fluctuating radial pressures displaced by the time lag τ

T is the time interval of integration.

This autocorrelation of pressures is similar to the lateral correlation between radial pressure components displaced in the direction of mean flow: the displacement distance is the product of the time lag and the mean flow velocity.

PERIODIC FUNCTIONS ANALYZED

Since most water pipe flow experimental measurements were of spectra, a brief theoretical discussion of harmonic analysis follows: it is a generalized Fourier series approach to the study of many functions. A Fourier series is an infinite series expression of a function that repeats itself over intervals of an infinite range of the independent variable. The function is expressed as an infinite series of constants multiplied by circular functions with periods of integer multiples of the period of the original function. The constant multipliers are obtained from the average of the function weighted by each harmonic circular function over the fundamental period, because of the important orthogonality conditions for circular functions. The function can be written in terms of the exponential form of circular or sine functions with both positive and negative angular velocities:

$$f(t) = \sum_{n=-\infty}^{\infty} F(n) e^{jn\omega_1 t} \qquad n = 0, \pm 1, \pm 2....$$

$$F(n) = \frac{1}{T_1} \int_{-T_1/2}^{T_1/2} f(t) e^{-j\omega_1 nt} dt \qquad (30)$$

where T_1 is the fundamental period $2\pi/\omega_1$

$f(t)$ is the periodic function expressed as an infinite series in $e^{-jn\omega_1 t}$

$F(n)$ is the complex constant of the series in $e^{-jn\omega_1 t}$
$f(t)$ and $F(n)$ are Fourier transforms of each other

$F(0)$ is the dc component which must be finite.

The autocorrelation of the periodic function $f(t)$ is obtained by the quadratic average:

$$R(\tau) = \frac{1}{T_1}\int_{-T_1/2}^{T_1/2} f(t)f(t+\tau)dt = \sum_{n=-\infty}^{\infty} |F(n)|^2 e^{jn\omega_1\tau} \tag{31}$$

where $|F(n)|$ is the absolute magnitude of $F(n)$

$|F(n)|^2$ is the power spectrum of $f(t)$

$R(\tau)$ is the autocorrelation for lag τ.

The autocorrelation and the power spectrum are Fourier transforms of each other:

$$|F_n|^2 = \frac{1}{T_1}\int_{-T_1/2}^{T_1/2} R(\tau)e^{-j\omega_1 n\tau}d\tau \tag{32}$$

Both the Fourier spectrum and the power spectrum are discrete functions of angular velocity. The function $f(t)$ is a periodic function of time, and the autocorrelation is a periodic function of the lag.

APERIODIC FUNCTIONS

Aperiodic functions such as transients are analyzed by the Fourier integral. The fundamental period of the Fourier series is allowed to approach infinity, and an aperiodic function is represented by the Fourier integral:

$$f(t) = \frac{1}{2\pi} \int_{-\infty}^{\infty} F(\omega) e^{j\omega t} d\omega$$

$$F(\omega) = \int_{-\infty}^{\infty} f(t) e^{-j\omega t} dt \qquad (33)$$

where $f(t)$ is an aperiodic function and the Fourier transform of $F(\omega)$

$F(\omega)$ is the Fourier transform of $f(t)$

$F(0)$ is required to be finite, the condition of convergence.

For aperiodic functions, the autocorrelation does not exist if it is defined as above, since it would be zero when averaging the quadratic over an infinite interval. The power spectrum does not exist but an energy spectrum does exist when the autocorrelation is defined as the quadratic sum without dividing by the period to form an average. The function $f(t)$ is aperiodic by definition, and the Fourier transform of $f(t)$ is a continuous function of frequency or angular velocity.

RANDOM FUNCTIONS

The water flow noise pressure fluctuations measured with the test hydrophones appear to be random functions of time. The autocorrelation function can be assumed to exist and be related to the power density spectrum. The autocorrelation is an even function with the maximum value for zero lag. For the autocorrelation function to be fully realizable, the power spectrum must be positive. Both the autocorrelation function and the power spectrum are real and even for random and periodic functions. The Fourier transforms for random functions can be written as cosine transforms:

$$R(\tau) = \lim_{T\to\infty} \frac{1}{2T} \int_{-T}^{T} p(t)p(t+\tau)dt = \int_{0}^{\infty} G(f)\cos\omega\tau df \qquad (34)$$

$$G(f) = 4\int_{0}^{\infty} R(\tau)\cos\omega\tau d\tau$$

where $G(f)$ is the power spectrum based on only positive frequencies

$R(\tau)$ is the autocorrelation

$p(t)$ is the wall pressure fluctuation.

Parseval's theorem is obtained by setting the lag equal to zero. This corresponds to the mean square value of the random function expressed in integrals both in frequency and lag as the independent variables:

$$R(0) = \overline{p^2} = \int_{0}^{\infty} G(f)df = \lim_{T\to\infty} \frac{1}{2T} \int_{-T}^{T} p(t)^2 dt \qquad (35)$$

where $\overline{p^2}$ is the mean square value of the random function.

The numerical integration of the measured power density spectra for water flow noise shows that they are equal to the broadband magnitude squared, as expected above. This shows that there are no hidden periodicies in the data.

FUNCTIONS SUMMARIZED

Some of the characteristics of the transforms are indicated by their dimensions. If the dimensions of $f(t)^2$ are assumed to be of the dimensions of power, the autocorrelations are of the dimensions of power. The power spectrum is in the terms of power times lag time, or work. The Fourier integral transform of a function $f(t)$ is of the

dimensions of $f(t)$ multiplied by time. The function $f(t)$ and autocorrelations must be aperiodic if their transforms (which are in the dimensions of a product with an infinite time interval) are to be finite. Random functions do not have finite Fourier transforms, but their autocorrelations are aperiodic and their power spectra are continuous functions. In the case of periodic functions, the autocorrelation and the power spectrum are in the same dimensions, as are the function itself and its Fourier transform. Here, the function and the autocorrelation are both periodic, and the Fourier spectrum and the power spectrum both occur at the same discrete frequencies. The nature of the transforms of various function types is summarized in table B-1.

TABLE B-1. NATURE OF TRANSFORMS OF VARIOUS FUNCTION TYPES

	FUNCTION TYPES				
TRANSFORMS	Periodic	Transient	Random	Step	Impulse
$f(t)$	periodic	aperiodic	continuous	continuing	discrete
Fourier spectrum	discrete	dc component continuous	infinite everywhere	infinite at zero dc component after step	continuous
Power spectrum	discrete	none (energy spectrum)	continuous	discrete at zero only	none
Autocorrelation	periodic	none	aperiodic	continuous	none

NUMERICAL ANALYSIS

AUTOCORRELATIONS

In the water pipe flow experiments, photographs were taken of oscilloscopic tracings of hydrophone signals, to provide time records of sound pressure at one point in the pipe for numerical evaluation of the autocorrelations and power spectra. The form of correlation coefficient for numerical data is the sum of the product of the differences from the mean values for the two variables divided by their magnitudes:

$$R = \frac{\sum (x-\bar{x})(y-\bar{y})}{\sqrt{\sum (x-\bar{x})^2 \sum (y-\bar{y})^2}} \tag{36}$$

where x and y are two variables correlated.

For the time data, the record is divided into N readings, x_r, $r=1, 2, 3, \ldots N$ equally spaced intervals, τ_1, with the time record, $T=N\tau_1$. The autocorrelation between the values of x_r at two points on the record is obtained for the lag time between them. The lag, τ, is taken as equal to $m\tau_1$, with $m=0, 1, 2, 3, \ldots K$ $K<N$. The autocorrelation as a function of the number of lag intervals, m, is given by.

$$R_m = \frac{\sum_{r=1}^{N-m} (x_r - B_m)(x_{r+m} - C_m)}{\sqrt{\sum_{r=1}^{N-m} (x_r - B_m)^2 \sum_{r=1}^{N-m} (x_{r+m} - C_m)^2}} = \frac{A_m - B_m C_m}{\sqrt{(D - B_m^2)(E - C_m^2)}} \tag{37}$$

where $A_m = \frac{1}{N-m} \sum_{r=1}^{N-m} x_r x_{r+m}$

$$B_m = \frac{1}{N-m} \sum_{r=1}^{N-m} x_r$$

$$C_m = \frac{1}{N-m} \sum_{r=m+1}^{N} x_r$$

$$D_m = \frac{1}{N-m} \sum_{r=1}^{N-m} x_r^2$$

$$E_m = \frac{1}{N-m} \sum_{r=m+1}^{N} x_r^2$$

$m=0,\ 1,\ 2,\ 3,\ \ldots\ K\ K<N$

If B_m, C_m, and E_m are essentially constant, the autocorrelation equation simplifies to the form:

$$R_m = \frac{A_m - \bar{x}^2}{x^2 - \bar{x}^2} \tag{38}$$

where $\bar{x} = \frac{1}{N} \sum_{r=1}^{N} x_r$

$$\bar{x}^2 = \frac{1}{N} \sum_{r=1}^{N} x_r^2$$

The power spectra were calculated by an equation that does not use the autocorrelations as computed above. The number of time data in the photos is small, even though several were combined in the analysis. The normalized power spectra were calculated by the equation equivalent to the numerical Fourier transform:

$$P_n = \frac{\tau_1 (u_n^2 + v_n^2)}{w}$$

$$u_n = \sum_{r=1}^{k} (x_r - \bar{x}) \cos 2\pi r f_1 \tau_1 n \tag{39}$$

$$v_n = \sum_{r=1}^{k} (x_r - \bar{x}) \sin 2\pi r f_1 \tau_1 n$$

where $w = k(x^3 - \bar{x}^3)$

$$f_1 = \frac{1}{2k\tau_1} \qquad f_n = nf_1$$

The power spectra at the frequencies corresponding to each n were smoothed by a Hamming method:
$\overline{p_n} = 0.23p_{n-1} + 0.54p_n + 0.23p_{n+1}$.

Figures 5 and 6 show the autocorrelations obtained by the numerical method from the photographs. The autocorrelation curves give, for the steady flow, the Taylor microscale defined by:

$$\frac{1}{\lambda_{t^2}} = -\frac{1}{2}\left[\frac{\partial^2 R}{\partial t^2}\right]_{t=0} \tag{40}$$

The integral scale is obtained from the integral:

$$\lambda_I = \int_0^\infty R\,dt \tag{41}$$

With uniform mean flow velocity $\bar{u}$, the time scale in the autocorrelations is equivalent to distances equal to the mean velocity multiplied by the time values. Approximate average values of the microscale and the integral scale are 0.075 and 0.11 inch, respectively.

MICROSCALES

Taylor measured the microscales of turbulence which he himself originally defined. His longitudinal velocity microscale is a function of flow velocity, being about 0.315 inch at 7.5 fps flow. The lateral velocity microscale is 0.707 of the longitudinal for isotropic turbulence. The longitudinal, or tunnel-direction, microscale has an average value of 0.15 inch for the broadband measurements at the U. S. Navy Underwater Sound Laboratory. The lateral, or cross-channel, microscale has an average value of 0.49 of the longitudinal average.

POWER SPECTRUM

Figures 9 and 10 show spectra numerically evaluated from the photographs by the procedures mentioned. Analysis of random functions is based on the assumption that all samples of the data have the same autocorrelation under the same flow conditions. The Wiener theorem states that the Fourier transform exists if the autocorrelation exists. The power density spectrum is the same for all waveforms. The power spectra were also calculated by the numerical form of the Fourier transform of the autocorrelations:

$$P_n = \tau_1 \left[1+2 \sum_{rm=1}^{k} R_m \cos 2\pi nm f_1 \tau_1 \right] \qquad (42)$$

$$m=1,\ 2,\ 3,\ \ldots\ k \qquad n=1,\ 2,\ 3,\ \ldots\ k$$

where P_n is the power spectrum

τ_1 is the chosen time interval

f_1 is the chosen frequency interval, $f_1 = \frac{1}{2k\tau_1}$.

The mean squared value of the pressure has been shown to be the autocorrelation for zero time lag, and the integral of the power spectrum:

$$\overline{p}^2 = \lim_{T \to \infty} \frac{1}{T} \int_{-T/2}^{T/2} p^2(t)dt = \int_0^\infty G(f)df \qquad (43)$$

where $G(f)$ is the power spectrum

f is the frequency

T is the time period.

ENERGY SPECTRUM

Graphs in this report show the square root of the power spectrum plotted against wave number. Much of the theory of turbulence has been concerned with the frequency distribution of kinetic energy. Pressure can be considered to be kinetic energy per unit volume, at least in dimensions. Thus, the square root of the power spectrum of pressure is of the same dimensions as the kinetic energy spectrum. Taylor first showed the transform relationship between the kinetic energy spectra and the correlations of the velocity components. His kinetic energy spectra were in terms of the one-dimensional wave number. The wave number is equal to the angular velocity divided by the mean velocity, and has the dimensions of an inverse length. Mathematical expressions for eddies are written in terms of three-dimensional wave numbers, and these are directly related to the eddy sizes. Large eddies cause fluctuations at low frequencies, and small eddies cause high frequency fluctuations. For the one-dimensional wave number, the inverse of the wave number cannot be directly connected with eddy sizes.

Figure B-12 indicates the general form of the kinetic energy spectrum plotted against wave number for isotropic turbulence. The lower wave-number range contains the largest eddies; these show permanence and depend upon the condition of formation. The energy spectrum is maximum in the range of energy-containing eddies. The reciprocal

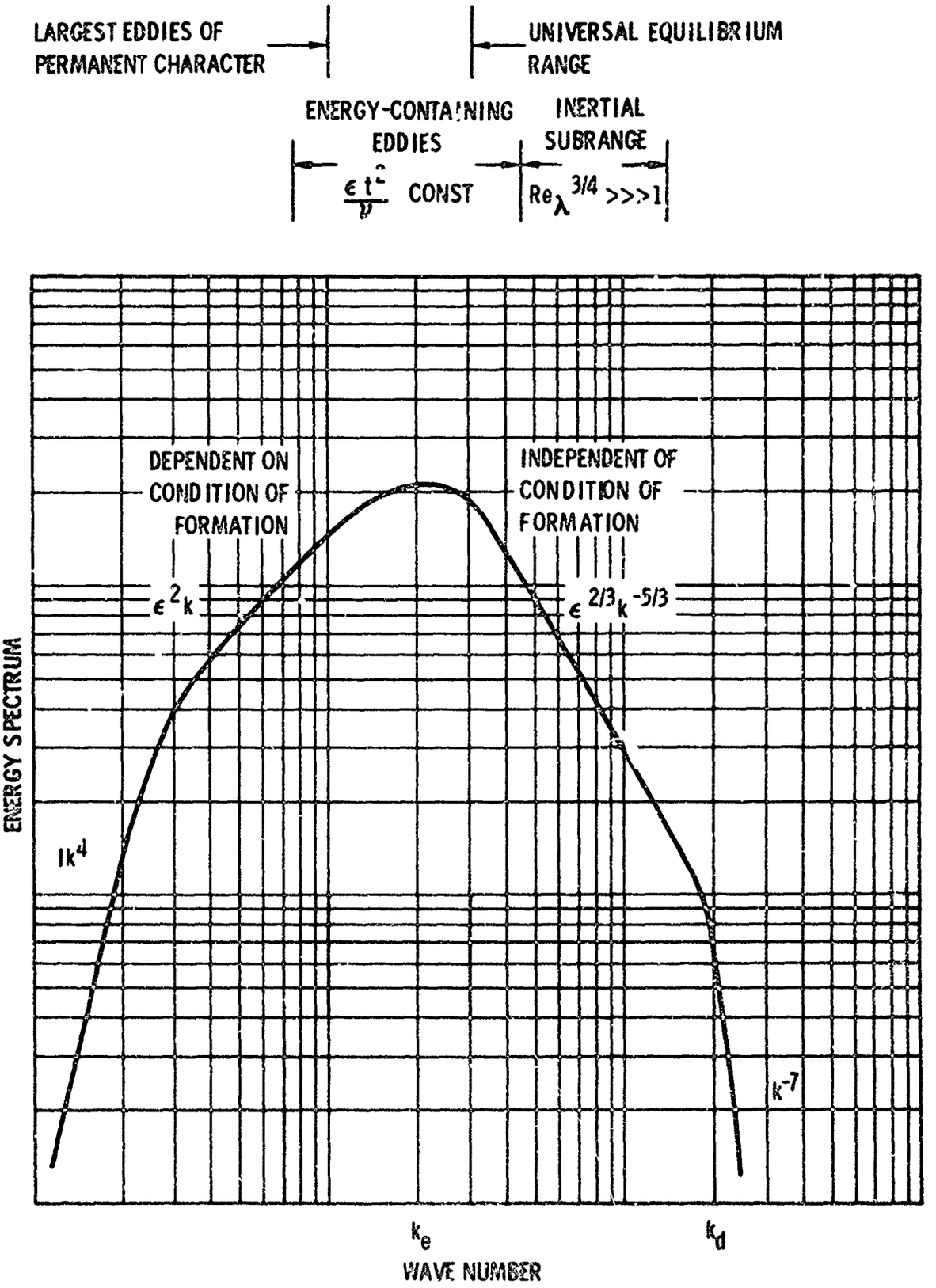

Figure B-12. Figurative sketch of energy spectrum levels, indicating relationships (adapted from ref. 2).

of the wave number of the peak energy is interpreted as the average size of the energy-containing eddies. In the highest range, the turbulence becomes statistically steady, with the change in the mean values becoming small with time.

In this Kolmogoroff range at sufficiently high Reynolds numbers, the turbulence is independent of external conditions and is in statistical equilibrium determined by the dissipation rate and the kinematic viscosity. There is an inertial subrange for very high Reynolds numbers where the energy spectrum is independent of the kinematic viscosity, and depends solely on the dissipation. The predicted slope of the energy spectrum/wave number plot in the equilibrium range is proportional to the negative 5/3 power of the wave number. Viscous effects become important as the wave number increases.